Co-assembly of graphene oxide / magnetic bimetallic nanoparticles for high-efficiency removal of tetracycline

Parnaz Tabrizian

A Thesis
In
The Department of
Building, Civil and Environmental Engineering

Presented in partial fulfillment of the requirement
For the Degree of Master of Applied Science (Civil Engineering) at
Concordia University
Montreal, Quebec, Canada.
April 2017

CONCORDIA UNIVERSITY

School of Graduate Studies

This is to certify that the thesis prepared

By: Parnaz Tabrizian

Entitled: Co-assembly of Graphene oxide and magnetic bimetallic nanoparticle for highly efficient removal of Tetracycline

and submitted in partial fulfillment of the requirements for the degree of

Master of Applied Science (Civil Engineering)

complies with the regulations of the University and meets the accepted standards with respect to originality and quality.

Signed by the final Examining Committee:

Dr. Catherine Mulligan
_____ Chair

Dr. Zhi Chen
_____ Examiner

Dr. Waiz Ahmed
_____ Examiner

Dr. Saifur Rahaman
_____ Supervisor

Approved by _____

_____ _____

Abstract

Co-assembly of graphene oxide / magnetic bimetallic nanoparticles for high-efficiency removal of Tetracycline

Parnaz Tabrizian

To prevent the human health risks presented by the rise of antibiotic resistant bacteria and the negative ecological impacts of large amounts of antibiotics entering the environment, it is crucial to develop effective technologies for the reduction and elimination of residual antibiotics in water.

Current conventional waste water treatment plants (WWTP) are not specifically designed to effectively remove complex organic molecules such as antibiotics. To address this problem many physical and chemical methods have been developed and tested for removal of antibiotics from environmental sources. However, these methods are highly condition based and potentially expensive. Recently, nanoscale zero-valent iron (nZVI) have gained a lot of attention for removal of wide range of organic and inorganic contaminants. It is recognized that nZVI tends to aggregate and oxidize rapidly, reducing the effectiveness and lifetime of these nanoparticles. To overcome these problems, several modification techniques have been developed. In this study, a novel magnetic nanocomposite based on the electrostatic interactions between graphene oxide (GO) and copper/iron bimetallic nanoparticles was prepared. In comparison to the previously studied "one pot, *in-situ*" preparation method of GO based nanocomposites, this co-assembly took advantage of the physical affinity between GO and bimetallic nanoparticles allowing for fine-tuning of the size and dimension of the nanoparticles prior to assembly. The nanocomposite showed a pH dependent assembly behavior that could be used to recycle GO and generate new nanoparticles. At optimal conditions, the novel nanocomposite demonstrated almost complete (~100%) removal of tetracycline (TC) within the first 20 minutes. Nanocomposite showed great performance for pH range of 3 to 8 (above 97%) with nearly complete removal for pH values 5 to 7. Desorption studies exhibited that the nanocomposite not only removed TC but also its transformation products. LC–MS analysis showed that the degradation products were mainly stemmed from TC after the losses of some functional groups from the ring. As well as a high removal efficiency, this nanocomposite showed high stability and easy separation, making it a

promising method for treating latent antibiotics in water.

Acknowledgments

I owe my deepest gratitude to my supervisor Dr. Saifur Rahaman, for granting me the opportunity to pursue my graduate studies at Concordia University. I really appreciate his motivation, enthusiasm and immense knowledge. I would also like to thank my colleagues in our research group for their support and encouragement. It was an honor to work with such an extraordinary and talented team.

Dedication

I would like to dedicate my thesis to my father who always believed in my potential and to my mother for her never ending support. I also dedicate this thesis to my family and Eric for standing by me in ups and downs.

Table of Contents

List of Figures

List of Tables

Abbreviation List

AC	Activated Carbon
AMR	Antimicrobial resistance
apoTC	Apotetracycline
BET	Brunauer–Emmett–Teller
BNP	Bimetallic Nanoscale Particles
CMC	Carboxymethyl Cellulose
CTC	Chlorotetracyline
DI	Deionized
DO	Dissolve Oxygen
EATC	Epianhydrotetracycline
EDS	Energy-Dispersive X-ray Spectroscopy
EIC	Extract ion chromatograms
ESI	Electro spray ionization
GO	Graphene Oxide
ICP-MS	Inductively Coupled Plasma Mass Spectrometry
JCPDS	Joint Committee on Powder Diffraction Standards
LC	Liquid chromatography
LOD	Limit of detection
LOQ	Limit of qualification
MDL	Method of detection limit
MF	Microfiltration
MS	Mass spectroscopy
NF	Nanofiltration
NP	Nanoparticle
nZVI	Nanoscale Zero-Valent Iron
PRB	Permeable Reactive Barrier
PZC	Point of Zero Charge

RO	Reverse Osmosis
TC	Tetracycline
TEM	Transmission Electron Microscopy
TIC	Total ion chromatography
TP	Transformation products
UF	Ultrafiltration
VA	Veterinary Antibiotics
VDW	Van Der Waals
WHO	World Health Organization
WWTP	Waste water treatment plant
XPS	Photoelectron Spectroscopy
XRD	X-ray Diffraction

Chapter 1: Introduction

1.1 Problem statement

In recent years, there has been a growing interest in occurrence, transport and fate of human and veterinary antibiotics in the environment. Antibiotics are a diverse range of compounds (natural or semi-synthetic) that possess antibacterial activities. Ever since the discovery of penicillin by Alexander Fleming, there has been hundreds of other antibiotics available on the market for use in human and animals. Antibiotics play a major role in agriculture and livestock industries. They are used as a medicine to combat diseases, as growth promoters in poultry and livestock and as an additive to improving feed efficiency. Most of these antibiotics excrete unchanged in the feces and urine of humans and animals. Given that land application of animal waste as fertilizer is a common practice in agriculture industries, there is a growing concern about the impact of these antibiotic residues in the environment [1, 2].

The most common and broad spectrum antibiotics used for veterinary purposes and human health are penicillins, aminoglycosides and tetracyclines [1]. Among the variety of pharmaceuticals used, tetracyclines rank as the most highly used group of antibiotics at 5.6 million kilograms per year, summing up to almost 42% of the total antibiotics used yearly for livestock production [3, 4]. Tetracycline was discovered in 1940s and has been used extensively ever since. [5]. Tetrarcyclines are a class of antibiotics including oxytetracycline (OTC), tetracycline(TC), demethylchlortetracycline, rolitetracycline, methacycline, doxycycline, minocycline, and recently tigecycline[5, 6]. Effective antimicrobial action and absence of major side effects has resulted in extensive use and production of these antibiotics for human and veterinary purposes [7].

Antibiotics used in the health care system and hospitals commonly end up in the influent of municipal waste water systems (WWTP). However, current treatment processes operating in WWTPs are not designed specifically to effectively remove pharmaceuticals and emerging contaminants and therefore, a part of these contaminants are discharged to the surface waters or reclaim waters used in agriculture. Removal efficiency of current conventional water treatment

for pharmaceuticals can range from 10 to 95% [2, 8]. Constant exposure of the environment to antibiotics can disturb natural biological processes and promote multi-antibiotic resistance bacteria. Emergence of resistance is a highly complex process which is not yet fully understood with respect to the significance of the interaction of bacterial populations and antibiotics, even in a medicinal environment. However, it is known that antibiotics at sub-inhibitory concentrations in environmental sources such as water or soil can have an impact on cell functions and change the genetic expression of virulence factors or the transfer of antibiotic resistance [9, 10].

In the last two decades, several methods have been developed to treat WWTP effluents or remediate contaminated environmental sources. Several physical and chemical degradation methods such as chemical oxidation, adsorption, membrane filtration, ozonation, photo-fenton, and biotic degradation methods such as activated sludge, membrane reactor, and fixed bed reactor treatment have been applied to many antibiotics including TC with the purpose of degrading them in environmental sources [10-13]. However, these methods are highly condition based and potentially expensive. Therefore, it is crucial to investigate novel methods to remove and remediate antibiotics in the environment. Recently nanotechnology has been introduced as an interesting alternative to traditional methods [14, 15].

Nanotechnology, which can be defined as a deliberate manipulation of matter less than 100 nm, takes advantage of the properties of material at small scales. High reactivity and high adsorption capacity of these nanomaterials is a direct result of the high surface area and abundant active sites for interaction with contaminants. Nanomaterials can be further manipulated to create adsorbents or catalyst with specific functional groups for higher reactivity and selectivity towards adsorption and degradation of contaminants. Recent research has highlighted various advantages of nanomaterial based methods in comparison to traditional methods. However, today the knowledge about the environmental fate, transport and toxicity of nanomaterials is very limited and must be taken into consideration [14, 16].

1.2 Objective

The purpose of this research was to assess the potential use of graphene oxide supported iron copper bimetallic nanoparticles for removal of tetracycline from aqueous solutions. To the best of author's knowledge deposition of Fe/Cu nanoparticles on graphene oxide nanosheets have never been studied. The author could not also find any publication for co-assembly (ex situ method) of bimetallic nanoparticles on a support. In this study, the following items were investigated:

1. Physical and chemical properties of synthesized nanocomposites
2. Performance evaluation of synthesized nanocomposite for removal of TC from water
3. Effect of experimental conditions on performance of the nanocomposite
4. pH responsive behavior of the nanocomposite
5. Stability of the nanocomposite
6. Identify transformation products and possible degradation pathway

1.3 Organization of dissertation

This dissertation comprises four sections ordered chronologically as they appear in the thesis.

Chapter 1: A short introduction including the problem statement and scope of the project
Chapter 2: Literature review on environmental impacts of antibiotics and potential of engineered nanomaterials as a remediation technique
Chapter 3: Materials and method section describing reagents and chemicals used in this study, synthesis of different nanomaterials and nanocomposites, sample preparation and method for characterization studies and finally experimental setup and conditions for performance evaluation studies.
Chapter 4: Results and discussion section reporting the characterization and performance results
Chapter 5: Conclusion and recommendations for future studies
And finally Appendix and list of references

Chapter 2: Literature review

2.1 Antibiotics origin, source and occurrence in the environment

Antibiotics can enter the environment as parent compounds or metabolites and degradation products from a variety of input sources. As mentioned before, there has been many attempts to extract and detect these compounds from different environmental matrices such as soil and surface waters, and with the development of sophisticated analytical methods such as liquid chromatography and mass spectroscopy, researchers have been able to detect and quantify antibiotics in the environment. Antibiotics can enter the environment from different input sources as shown in Figure 2-1.

Most importantly, antibiotics used as veterinary medicine and growth promoters will be excreted from livestock unchanged (25-75%). For example, it was found that 40-80% of oxytetracycline administered to livestock feed is excreted unchanged.[17] After a period of storage, these excretes are applied to agricultural land field as a liquid manure that consists of feces and urine of livestock with high levels of antibiotics as a fertilizer. Therefore, antibiotics will be introduced to the soil matrix. In a two-year liquid manure application study by Hamscher et al. [18] they found that the rate of tetracycline accumulation exceeds the rate of antibiotic degradation resulting in accumulation of tetracycline overtime. They reported the amount of 4.0 and 0.1 mg kg^{-1} of tetracycline and chlorotetracycline in liquid manure and concentration of 86.2 μg kg^{-1} in the top soil levels up 10 cm. Counterintuitively, higher concentrations of 171.7 μg kg^{-1} were detected in deeper levels of soil (20-30 cm) [3, 18].

When introduced to the soil matrix, these antibiotics can leach or run off to surface waters. Similarly, human antibiotics can enter the sewer network and end up in WWTP. As mentioned before, most waste water treatment plants are not designed to efficiently remove micropollutants such as antibiotics. Therefore, a portion of these antibiotics will end up in surface waters and leach to ground waters.

Another major input source of antibiotics is the improper direct disposal of unused or expired medicine which is directly discharged in the sewage network or landfills. Waste effluents from hospitals or factories also contain high concentrations of antibiotics and can be considered as one of the major contributors to the release of antibiotics in the environment. Other sources can be accidental spills during manufacturing or distribution of antibiotics. A summary of the exposure pathways are shown in Figure 2-1.

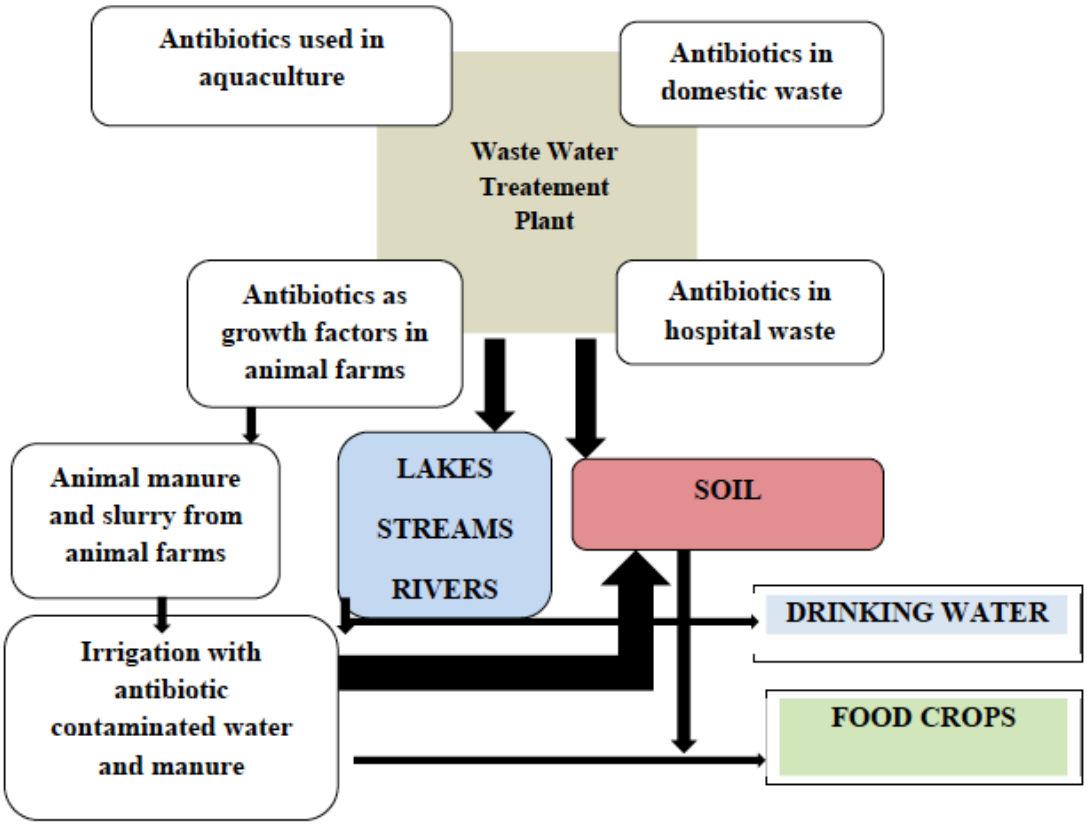

Figure 2-1: Antibiotic exposure pathways and entry to different environmental resources [19]

2.2 Tetracyclines and tetracycline chemistry

Tetracyclines (TCs) are broad-spectrum antibiotics meaning that they act against a wide range of gram-positive and gram-negative bacteria diseases such as chlamydia, urinary tract, respiratory tracts and intestine. However, the effectiveness of tetracycline has been reduced due to antibiotic

resistance. They are still used for a variety of human purposes and are used widely as veterinary antibiotic. Tetracycline is a family of antibiotics collectively referred to as tetracyclines, includes chlortetracycline (CTC), oxytetracycline (OTC), tetracycline (TC), demethylchlortetracycline (DC), rolitetracycline, methacycline, doxycycline, minocycline, and tigecycline.

Tetracycline as the name suggests has four conjugated carbon rings (tetracycle) with a carboxyamine functional group. Tetracycline has several ionizable functional groups and therefore, charge of the molecule depends on the pH of solutions. The summary of disassociation constants for the main tetracycline species is shown Table 2-1.

Table 2-1: pKa values for TC species in aqueous solutions at 25°C

	pK1	pK2	pK3
TC	3.3	7.8	9.6
OTC	3.2	7.5	8.9
DC	3.0	7.9	9.2
CTC	3.3	7.6	9.3

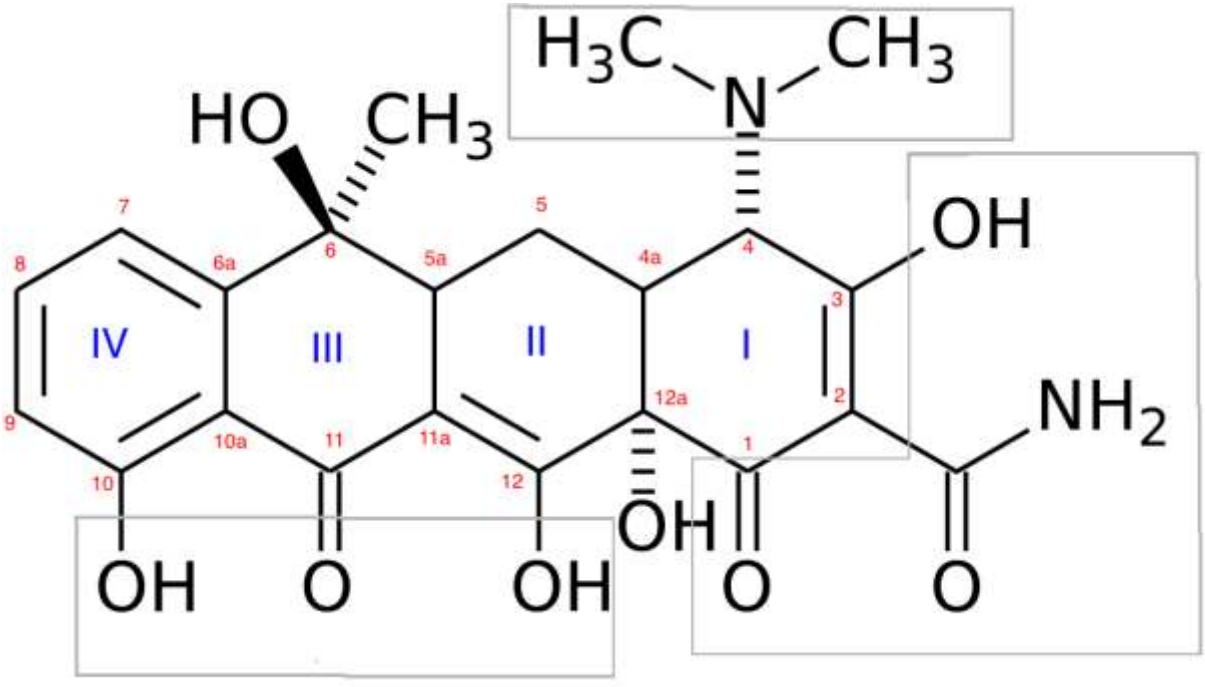

Figure 2-2: Molecular structure of TC showing 3 distinct ionizable functional groups

Molecular structure of TC is shown in Figure 2-2. The three distinct functional groups for TC is 1) tricarbonyl ammonium (pK_a 3.3); 2) phenolic diketone (pK_a7.7); and the dimethyl ammonium cation (pK_a 9.6). This structure suggests that TC is a cation (+ 0 0) in aqueous solution with pH lower than 3.3, a zwitterion for pH values between 3.3 and 7.7 (+-0) and an anion (+ - -). Chemistry of TC is an important for determining the electrostatic interaction between TC species and catalysts or adsorbent. Most waste water samples have a pH range of 4 to 8, in this pH range TC is in a zwitterionic form. In general TC species are stable in acidic conditions but not in alkaline conditions [17].

Tetracycline has 4 epimers, in the pH range 2-6 since strong pH conditions facilitates dehydration of hydrogen. In TC's case this isomerization occurs with dehydration of hydrogen at position C5a and C6. Resulting in formation of anhydrotetracycline (ATC), epianhydrotetracycline (EATC), apotetracycline (apoTC) and terrinolide. Isomerization must be considered during liquid chromatography studies since at lower pH TC can isomerize and have a different retention time than TC at neutral or alkaline pH.

It is important to point out that TC can easily complex with different metal ions such as Fe^{3+}, Fe^{2+}, Cu^{2+}, Mn^{2+}, Ca^{2}+ etc. Tetracycline can form chelate complexes with their ketoenolate moiety at ring 2 and 3. This complexing behavior can affect UV spectral band resulting in a dramatic peak shift. Analyzing liquid chromatography and mass spectroscopy (LC/MS) results can be very challenging with TC complexing behavior resulting in coexistence of multiple species of chelated TC present in the solution as well as ternary complexes (TC+metal+ligands). [19, 20]. This complexing behavior is also important for studying the leaching behavior of TC into deeper levels of soil. Strong affinity of TC to components of topsoil makes it improbable that TC leach into subterraneous water bodies and is rather present in superficial water. Cations of heavy metals such as Cu^{2+} have a large effect on mobility of tetracycline in the soil and can increase adsorption of TC to adsorbents [21-23]. A summary of physio and chemical characteristics of tetracycline is shown in Table 2-2.

Table 2-2: Summary of physio-chemical characteristics of tetracycline

Name	Tetracycline
Chemistry name	4(dimethylamino)1,4,4a, 5,5a,6,11,12aoctahydro3,6,10,12,12apentahydroxy6methyl1
Formula	$C_{22}H_{24}N_2O_8$
Molecular weight	444.44 g/mol
CAS number	60-54-8
Appearance and odor	Yellow crystalline powder, odorless
Solubility	Freely soluble (10 mg/ml), freely soluble in alkali hydroxide and carbonates solutions; sparingly soluble in alcohol; practically insoluble in chloroform and in ether.
Stability	Is stable in air, but exposure to strong sunlight causes it to darken. It loses potency in solutions of pH below 2 and is rapidly destroyed by alkali hydroxide solutions.

2.3 Environmental impact of antibiotics

As mentioned previously, even low levels of antibiotic in the environment can cause significant damage to the biota and cause antimicrobial resistant (AMR). AMR has become such a dire issue that United Nations (UN) held a high-level meeting on September 2016. This meeting that only deals with high stress issues such as war and economics has been held only 3 other times for health topics (HIV, non-communicable diseases and Ebola). This meeting is a clear recognition of worldwide issue that has been alarmed for many years by the World Health Organization (WHO). [24]. United Kingdom (UK) has prepared a report regarding the economic implications of antimicrobial resistance in the environment. In this report, it has been suggested that AMR can be the major cause of death in 2050 with projected 10 million deaths per years resulting in more than 100 trillion USD of GDP loss by 2015. It has been suggested by the report that this crisis can be averted if the world act immediately. Figure 2-3 shows the projected death rate caused by AMR in 2050 [25, 26].

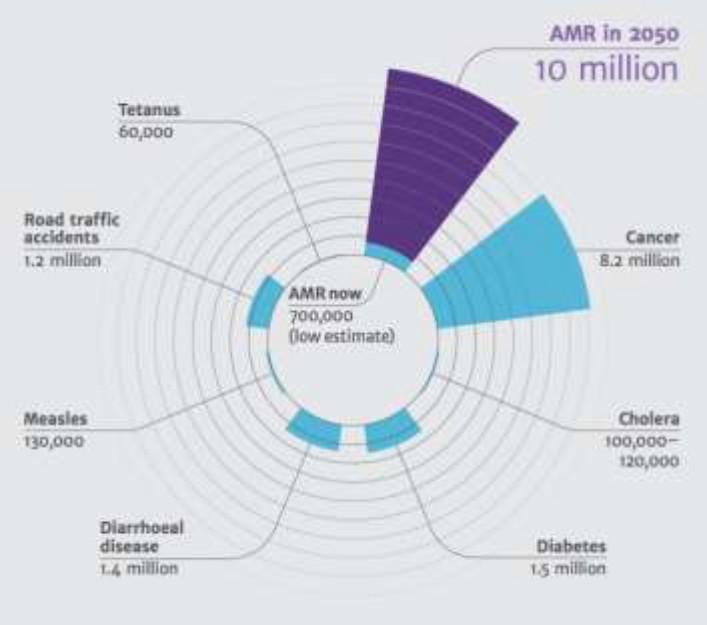

Figure 2-3: Current major causes of death and projected death by AMR in 2050 [26]

Antibiotic resistance is not a new phenomenon and is a natural revolutionary process. Resistance in bacteria can occur naturally and it has been associated with some strains of bacteria. Most bacteria species multiply rapidly enough to double their population every 20-30 minutes and therefore unfavorable condition will result in development of mutations for surviving under environmental stress [11]. Development of resistance is a complex process and not fully understood, but it is known that antibiotics at sub-inhibitory concentrations can alter the cell functions and change the genetic expression of virulence factor or the transfer of AMR. Antibiotic resistance can be a result of horizontal gene transfer and unlinked point mutations in pathogen genomes. AMR can also be passed along from mutated bacteria to their offspring which leads to microevolution of colonies of bacterial that are resistant to a drug or several drugs [27].

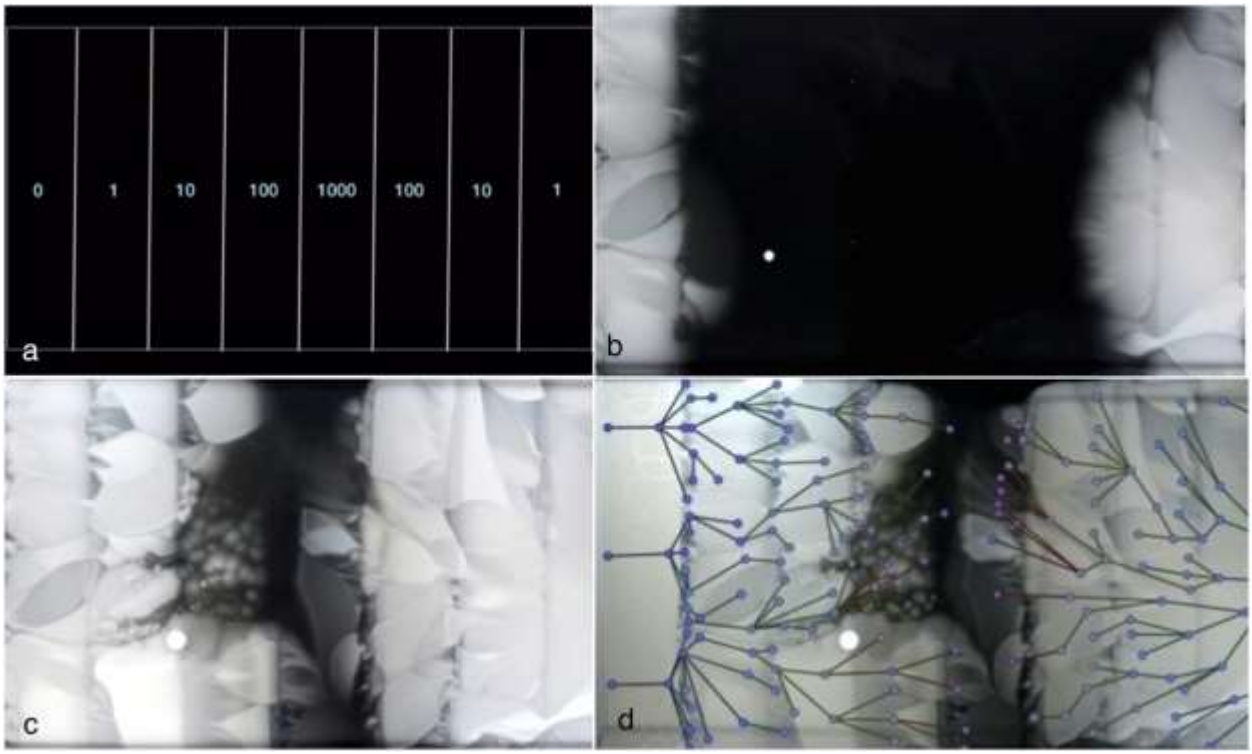

Figure 2-4: : Developed Mega-plate for visualization studies of microbial adaption a) setup of four-step exponential concentration rising of antibiotic on the mega-plate b) 44 h incubation c) 12 day incubation showing the growth of bacteria on the plate d)repeated mutation can be seen on the mega-plate [24]

Figure 2-4 shows a mega plate developed by Baym et al. [24] at Harvard University. This study motivated by the emergence of AMR, studied the mutation of *E-coli* in spatially distinct regions with varying concentration of antibiotic trimethoprim (TMP). After a 12-day incubation, a colony of *E-coli* was formed at concentrations of 100 times the inhibitory levels of this antibiotic. Although this study is not representative of the natural environment, it demonstrates how bacteria can adapt and form colonies in concentrations much higher than inhibitory levels with exposure to residual sub-inhibitory levels of antibiotics.

There are 3 proposed mechanisms in which the presence of antibiotics in the environment can potentially cause AMR related health issues to humans:

1) Direct infection with resistant bacteria from plant, water and animal sources
2) Breaches in species barriers by sustained transmission of resistant bacteria in live stock
3) Transfer of resistant genes from agriculture into human pathogens [28]

The first mechanism is a better-known mechanism comparing to the second and third mechanisms. The transfer of resistant bacteria to humans can occur via water, plants and meat. A plant that has been watered with surface water or fertilized by manure and a meat from an animal containing those strains of bacteria can infect the human population directly.

As well as contributing to AMR, antibiotics in the environment can exhibit ecotoxicity to the biota. Prolonged effect of exposure of low dose antibiotics and their metabolites on ecosystem is not known, however few studies has attempted to study the effect of antibiotic residuals on microorganisms in controlled laboratory conditions. Kummerer et al. [11] evaluated toxicity of TC and other major antibiotics to the strains of *Vibrio harveyi*, they have not found any toxicity effect for concentrations present in the environment but they have observed a decrease in reproduction comparing to the control experiment. A more extensive research by Kim et al. [29] studied the effect of TC on reproduction, size and morphology of *Daphnia magna,* observed 30 to 60% decrease of population growth rate with increasing concentrations of TC as well as increased size of *D. magna*. Overall, they reported inhibited propagation of this species in the long term.

Bioaccumulation is another aspect of pollutants in the environment. Bioaccumulation of organic compounds in the lipids of organisms typically occurs for organic compounds with octanol-water partition coefficients (K_{ow}) higher than 4.0. According to Regitano et al. bioaccumulation of antibiotics is not likely to occur since most of the antibiotics have a K_{ow} less than 4.0 and present in low concentrations in the environment. The same conclusion was made by Zhaeo et al.[30] to quantify the levels of human and VA antibiotics in specific tissues of wild fish. Although they found that digestion tissues, fish bile, plasma, and liver have strong bioaccumulation capacity towards some antibiotics, they reported that it is unlikely that consumption of these fish pose an appreciable risk to human health. Topal et al. [31] studied bioaccumulation of TC in *Lemna gibba l.* and observed 123 ppb accumulation in these species. Kim et al. [29] reported a whole body concentration of TC in algae (*P.subcapitata*) of 7 ng mg^{-1} when exposed to 1 mg L^{-1} of TC.

2.4 Antibiotic contaminated wastewater remediation

As mentioned previously, most conventional WWTPs and drinking water treatment plants (DWTP) are not designed to effectively remove antibiotics and pharmaceuticals. As a result, a portion of these pharmaceuticals could survive treatment processes and enter the environment via effluent from WWTP in a dissolved form or sorbed to the sewage sludge. For example, Ding et al. [7] extracted 15 target pharmaceuticals from biosolids and recovered 49-68% of TC from biosolids, proving the ineffectiveness of wastewater treatment towards pharmaceuticals.

Consequently, a wide range of chemical and physical methods has been used as a secondary or tertiary treatment to increase the removal efficiency of these antibiotics. Physical and chemical methods such as chemical oxidation, adsorption, membrane filtration, ozonation, photo-fenton, reverse osmosis (RO), and biotic degradation methods such as activated sludge, membrane reactor, and fixed bed reactor treatment have been applied to many antibiotics including TC with the purpose of degrading them in environmental sources.

Among conventional treatments, the biological processes, filtration and coagulation/flocculation/ sedimentation are the most used in conventional wastewater treatment plants. In biological treatment or conventional secondary treatments used by most WWTPs, conventional activated sludge (CAS) is used for removal of contaminants. The two main mechanisms of removal for antibiotics are biodegradation and adsorption. Most studies reported adsorption as the main mechanism of removal for 7 out of 11 antibiotics. The adsorbed portion can eventually reenter the environment and the microbial degradation can form products that are as active or potentially more toxic than parent compounds. Although this method can be applied to large effluent flow rates, most of these antibiotics are toxic and recalcitrant to the microorganisms of activated sludge therefore limiting the applicability of these processes [32].

In coagulation/flocculation process, chemicals such as trivalent salts or polymers are added to decrease the stability of suspended solids and eventually agglomeration and precipitation of suspended solid portion. In this method, there is a need to subsequently treat the pollutants in the coagulated form from the effluent and the dissolved portion of antibiotic will remain untreated.

Over all, most conventional techniques are proven to have low efficiency especially in high toxicity pollutant. Adams et al. [33] investigated the efficiency of traditional methods such as filtration, coagulation and clarification and the results showed low removal of antibiotics with maximum removal efficiency of around 30%. Therefore, due to low efficiency and sometimes impractical application of these methods, other techniques were developed and tested [32, 33].

In the chlorination process, which is the addition of chlorine or hypochlorite is currently a post treatment plant in WWTPs. However, this method is also used as an oxidation technique in removal of some pharmaceuticals and transforming them to less toxic compounds. Adams et al. [33] reported formation of chlorinated oxidation products such as chlorotetracycline. These products can be potentially more toxic than the parent compound. Ozonation is another oxidation technique commonly used for removal of pharmaceuticals. In this method ozone which is a strong oxidant is introduced to the system and has the advantage of versatility in terms of flow rate and pollutant composition. This method is costly and highly pH dependent and does not seem to be to an efficient option for removal of antibiotics.

Photolysis which is implementing natural or artificial light for the degradation of chemicals is another commonly used method. Photolysis performance is highly dependent on the adsorption spectrum of the target compound, radiation intensity. Natural wastewater can contain other substances that inhibit the process. Overall, photolysis is less effective than other methods. TC is highly light sensitive and Jiao et al. [34] reported 80% removal of TC but only 14% TOC removal. In their study, they also found that the toxicity of by-products is higher than the parent compound. This method is relatively ineffective comparing to other methods and not a great candidate for removing antibiotics [32].

Electrochemical processes are highly versatile, cost effective and a clean technology for removal of toxic organic compounds. In this method, oxidation occurs over an anode in the presence of an electrolyte. This method could degrade chemicals directly by anodic electrode exchange or indirectly in the liquid bulk by mediation of strong oxidants. Although this method seems like a promising processes for removal of high concentrated antibiotics, efficiency of this method is highly condition based and is limited to small flow rates [32].

Membrane based processes such as reverse osmosis, is usually applied for removal of large molecules in liquid effluents via diffusion method by applying high pressure. Adames et al. [34] investigated the removal of antibiotics via reverse osmosis and obtained high removal (>90%) for some antibiotics but 50-80% for TC and 11-20% for sulphonamides. Regardless of removal efficiency this method is very energy intensive and fouling of the membrane is a major issue. Moreover, the presence of other contaminants, salts or organic matters can inhibit the process [32].

Ion exchange is another process in which cations and anions in a liquid medium are exchanged with cations or anions on a solid sorbet. In addition to typical disadvantages of this method such as the necessity of backwashing and regeneration of sorbent, Adams et al.[34] reported the ineffectiveness of this method for antibiotic. Choi et al. [35] used polymeric resins for removal of TC and sulphonamides and reported more than 80% removal of TC but they also reported the interference of organic compounds as the major problem associated with this method [33, 35].

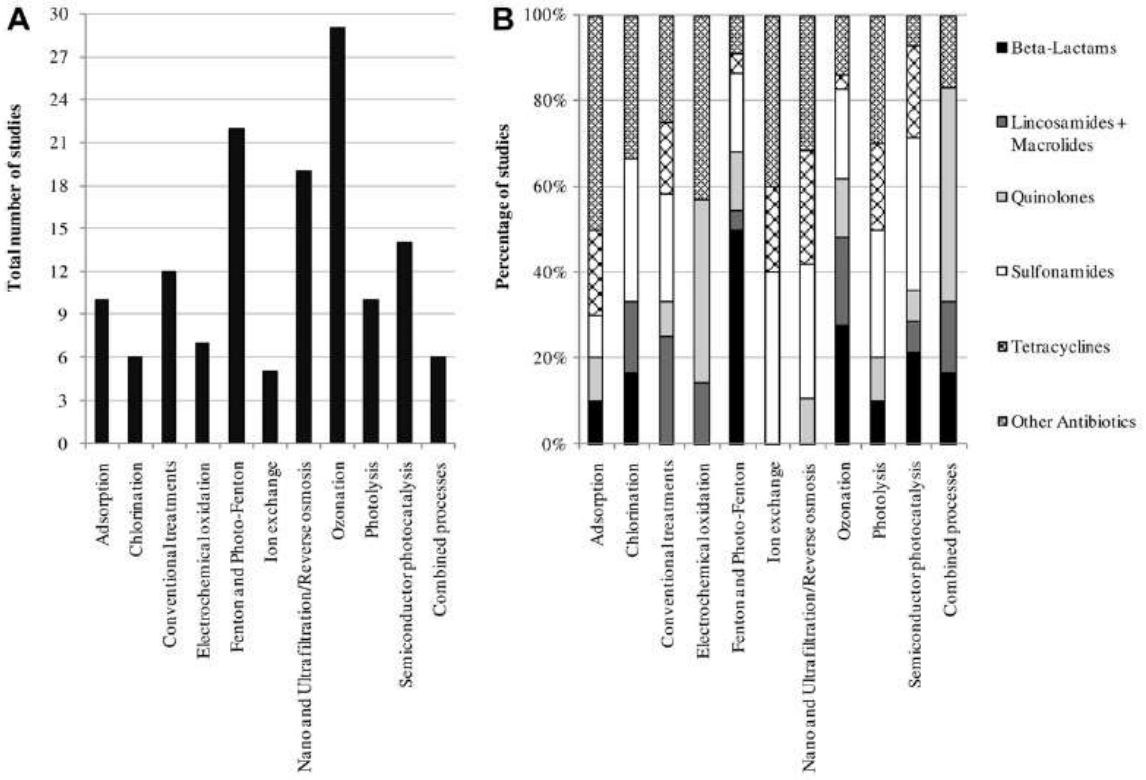

Figure 2-5 A) Comparison between the most studied methods (B) and the most applied methodology for each class between the years 2000 and 2010 [30]

In summary, failure of conventional WWTP treatment plant in efficient removal of antibiotics creates the need for application of other methods. Figure 2-5 summarizes the current studies performed on different class of antibiotics. From this graph, it is evident that filtration, adsorption and photocatalysis are the most commonly applied method for removal of TC regardless of their limitations. To date, a more feasible and promising strategy in removal of antibiotics are a combination of previous techniques. However, recent studies which created and applied nanomaterials as potential catalysts and adsorbents for removal of recalcitrant chemicals such as antibiotics attracted a lot of attention.

Among these adsorbents, magnetic nanoparticles with the ability to easily separate from the aqueous media are gaining a lot of attention since they are highly efficient, inexpensive and non-toxic. Magnetic nanoparticles (nZVI or Fe_3O_4) have been widely studies for removal of pollutants such as chlorinated compounds, dyes, heavy metals and pesticides. nZVI degradation of TC have been reported by Hanay et al. [35] and Chen et al. [36, 37].

2.5 Iron nanoparticles and modification techniques

Nanoscale zero-valent iron (nZVI) and iron oxide nanoparticles are one of the most extensively applied nanoparticles for removal of pollutants and environmental remediation. nZVI is the most commonly used nanomaterial in Europe and United States for soil and groundwater remediation. Small size, high reactivity towards a wide range of contaminants, high adsorption and reductive potential and low cost production of these NPs make them an idea candidate for environmental applications in different matrices. nZVI has been extensively researched and used for removal of of inorganic and inorganic contaminants such as halogenated compounds, pharmaceuticals, nitrate, phosphate, dyes and heavy metals (Ni^{2+}, Co^{2+}, Cu^{2+}).

There are many methods for large scale production of iron NPs such as milling, chemical reduction, green synthesis, ultrasound or electrochemical method. These methods are either using a top-down approach such as mechanical grinding of microscale iron or bottom-up approach by

reduction of sulfate or chloride salt of iron metals. In the first approach the particles exhibit a high surface energy and thus are more prone to aggregation.

Although iron nanoparticles are effective for a range of organic and inorganic contaminant removal, there are several drawbacks associated with iron NPs such as rapid oxidization, aggregation and limited mobility. For any NP, key essential properties for environmental applications are 1) high reactivity for contaminant removal; 2) low toxicity; 3) sufficient mobility in porous media; 4) longevity. For iron NPs with high reduction potential, they can easily donate electrons and become oxidized to 2^+ and 3^+ oxidation states and in turn reduce organic compounds. However, they can also react with oxygen in aqueous media and thus lose their activity towards contaminants. Moreover, magnetic and electrostatic forces between iron NPs will result in aggregation of these NPs and thus they lose their reactive sites and mobility. To overcome these limitations, several modification methods have been developed. These methods can be categorized into five main methods, 1) coating the surface with stabilizing compounds; 2) other metal doping; 3) matrix encapsulation; 4) deposition of NP on a support [38]. A schematic summary of these methods are shown in Figure 2-6.

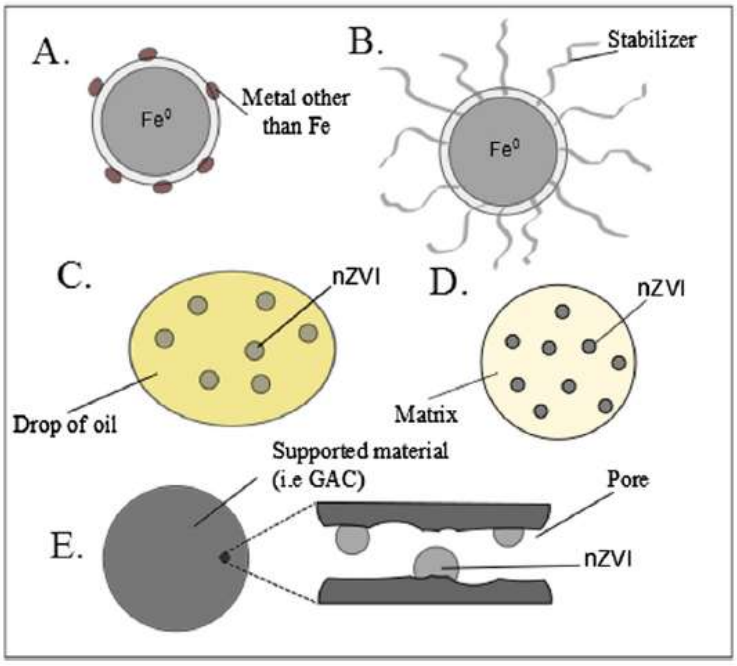

Figure 2-6:nZVI modification methods A) doping with other metals B) coating with stabilizers C) emulsification D)matrix encapsulation E)Depositing on support[36]

The first method, which is coating the surface of nZVI with surfactants or polyelectrolytes, is one of the main approaches aimed at increasing nZVI dispersion in aqueous media and increasing mobility in porous matrix. Surface coating changes the surface charge of nZVI and therefore changes electrostatic interaction between molecules preventing aggregation in nanoparticles. It was observed that nZVI coated with polyelectrolytes such as polyasarate, carboxymethyl cellulose (CMS) and polystyrene sulfonate can remain mobile much longer than the bare nZVI. Hydrophilic biopolymers such as starch, guar gum, alginate and aspartame have also been studied and proven effective [39-41]. Chen et al. (2015) coated nZVI with water-soluble, environmentally friendly and low-cost polyvinylpyrrolidone (PVP-K30) reported an almost 100% removal of 100 ppm TC from aqueous media [37].

A very well-known method for improving properties of nZVI is other metal doping. Addition of other metals to iron NPs especially doping of magnetic nanoparticles with noble metals have attracted a lot of interest and are proven to be a promising method to overcome the limitation of nZVI or improve remediation or catalytic properties through synergistic effects. Small amounts of metals such as Pd, Pt, Ag, Cu and Nickel can increase the activity of the resultant particles and provide good protection against oxidations. For example, Pd can make a significant increase in activity of nZVI for dehalogenation of chlorinated compounds. This method that results in nanoalloy or bimetallic nanoparticles has proven effective in removal of contaminants within aqueous matrix. This bimetallic NPs (BNPs) which are composed of two distinct metal elements, perform not only a simple combination or enhancement of properties of a simple element, but also can show surprising new properties with combination of multiple functions and broadened application. These nanoparticles can have different structures and geometrical patterns. The mixing patterns and elemental distribution of these NPS can be categorized into three main groups for zero dimension NPs; 1) core-shell b) dumbbell and C) alloyed [42].

In the core-shell structure there is a clear interface between the core and shell of the nanoparticle, having an element in the shell and another metal surrounding the shell. In the second category, metals form in an axial direction with distinct clusters resembling a dumbbell structure, sharing a

mutual interface. In the last category, metal elements are mixed randomly or in an ordered manner, in this structure presence of both elements on the surface can lead to a great catalytic activity of these NPs [42].

BNPs can be synthesized in a variety of ways which can be classified into two main categories: co-reduction method and sequential reduction method. In the sequential method, BNPs can be synthesized by soaking the freshly prepared nZVI consisting of a noble metal ion, reducing the noble metal and subsequent deposition of the other metal on the Fe surface. In another method, freshly prepared nZVI is soaked in a metal salt solution. If the standard reduction potential of doping metal is higher than iron, the metal will be reduced by iron through metal replacement reaction and deposits on the surface of the nZVI. Another common approach is co-reduction (one pot) method of the iron and the other metal. In this approach iron metal salt and the additive metal salt are reduced simultaneously by sodium borohydrate resulting in a different distribution and dispersion of elements of the BNPs[43].

Regardless of the structure of NPs, they have been proven effective with broad applications. For example, He et al. [40] reported selective hydrogenation of diethyl malonate to diethyl malonate by Cu/Fe-SiO_2 NPs. They observed that addition of appropriate amounts of Fe species enhanced the reduction of Cu^{2+} species, thereby increasing the Cu^0 species on the surface of bimetallic catalyst [43]. Tee et al. [44] reported an increase in the reaction rate of TCE degradation by Fe/Ni by two orders of magnitude higher than nZVI. Other researchers reported a complete degradation of TCE by Fe/Pd NPs in comparison to nZVI resulting in different end products [35, 44, 45].

Although BNPs have much greater reactivity and stability in comparison to nZVI, their short lifetime resulting from surface passivation or agglomeration might be still present. Moreover, introducing possible hazardous heavy metals pose more risk in environment. As a result, some researches employed other techniques to overcome these drawbacks. From these methods, depositing the BNPs on the solid surface is of particular interest. There has not been much research focusing on BNPs deposited on a support but the potential advantages associated with this method makes it a promising candidate.

Deposition of NPs and BNPs on a support has been one of the successful modification practices. Depositing NPs on a solid matrix such as silica, graphene, zeolites and polymer membranes can facilitate NP separation from a purified matrix as well as decreasing agglomeration and surface passivation. Deposition can be done (in situ or ex situ), in the in-situ method, also known as co-precipitation method, the iron salt and the support are in one solution and the sodium borohydrate is introduced in the system resulting in often uniform chemical deposition of NPs on the support. In the ex situ method, fresh synthesized NPs are mixed with pristine or modified support and the electrostatic interactions as well as other possible forces result in assembly of the NPs on the support. Ex situ method allows for tuning the size and characteristics of NPs before the deposition and a reversible pH sensitive assembly allows for recycling and regenerating the NPs. There have been also reports of synergistic effects between a support and the NPs [34, 46, 47].

Jiao et al. [34] studied the co-assembly of sulfonated GO and iron oxide nanoparticles for removal of organic dyes. They reported a nearly 100% removal for both freshly prepared and recycled nanohybrids, stating tunable dimensions and increased GO surface area as the advantage of co-assembly method. Liu et al. [46] deposited nZVI on a GO support for removal of diluted antibiotics. In this study, they used an interesting approach to take advantage of the reversible mechanism of this assembly for adsorbent regeneration and complete degradation by ozonation. GO supported nZVI showed almost complete removal of antibiotics for 9 cycles. They also reported a decrease in the formation of Fe^{3+} on the surface of nZVI after 2 day of aging, concluding that GO support reduced passivation of the NPs. Lam et al. [48] reported a remarkable effect of MCM-41 support on copper NPs in terms of distribution and loading rate of the NPs, the same author, investigated the Fe/Cu NPs supported on MCM-41 for degradation of Orange II dye and reported a reduction for activation energy of the reaction in comparison to the previous monometallic supported catalyst.

In addition, Zubir et al. [47] studied different possible structures of iron oxide NP loaded GO for different loading rates of GO. They reported that strong Fe-O-C bond of anchored NPs resulted in 20% higher degradation of Acid orange 7 than the unsupported NPs, claiming the synergistic

structure of GO-iron oxide under low loading rate of GO. In the later research (Zubir et al. [49]) the author reported that GO enhanced the incorporation of zinc into the iron oxide and limiting the crystal growth resulting in smaller crystal particles. They also reported that GO-Fe-ZnO showed 670% higher degradation of Acid orange 7 in comparison to the conventional heterogeneous reaction.

2.6 Graphene Oxide Nanosheets as a support for NPs

As mentioned before, aggregation of NPs and BNPs results in loss of mobility and reactivity of these nanoparticles. In order to reduce the aggregation, immobilization on a solid matrix can help preserve their activity for longer time. In the past few years, carbon materials show a great potential. Various carbonaceous materials such as activated carbon (AC), carbon aerogels, carbon microfibers, carbon nanotubes (CNT), mesoporous carbon and graphene have been used as a support for adsorbents and catalysts. Recently, graphene oxide (GO), a two-dimensional monolayer sheet of carbon atoms, has been considered as a great support because of abundant functional groups.

GO is a novel two-dimensional single layer carbon nanomaterial and is synthesized via strong oxidation of graphite via Hummer method. GO has unique properties associated with large quantities of oxygen atoms in the form of epoxy, hydroxyl and carboxyl groups, making GO extremely hydrophilic. GO is easily dispersible in water and a range of organic solutions, providing the ability to apply in aquatic and biological environment. GO possesses a high specific area (2630 m^2 g^{-1}). GO is chemically stable enough to be subjected to oxidative-degradation over a wide pH range, making it a suitable candidate for long-lived recyclable adsorbents and catalysts. Moreover, GO by itself has high adsorption capacity for a range of organic and inorganic contaminants [46, 50].

Several authors reported the synergistic effect of using GO as a support for adsorbents, suggesting that the adsorption properties of GO enable the pre-concentration of pollutants to be within the vicinity of the catalyst or adsorbent therefore, enhancing the activity of these

supported nanocomposites. In addition, abundant oxygen containing functional groups can facilitate a strong anchoring and uniform distribution of NPs on the GO surface [47, 48].

Regarding anchoring of NPs on the surface of GO several strategies have been reported. These methods are either in-situ or ex-situ. In the in-situ method which involves coordination or intercalation of metal NP species within the GO matrix and their subsequent growth and the ex-situ method which involves the preparation of NPs with specific dimensions and morphology prior to deposition on the GO surface, the former method has been widely studied and can adapt to many chemical processes that include hydrothermal and solvothermal synthesis. The ex situ method on the other hand, can be reversible and has the potential for allowing the regeneration and reuse of GO in a dynamic system [51]. Molecular structure of GO is shown in Figure 2-7.

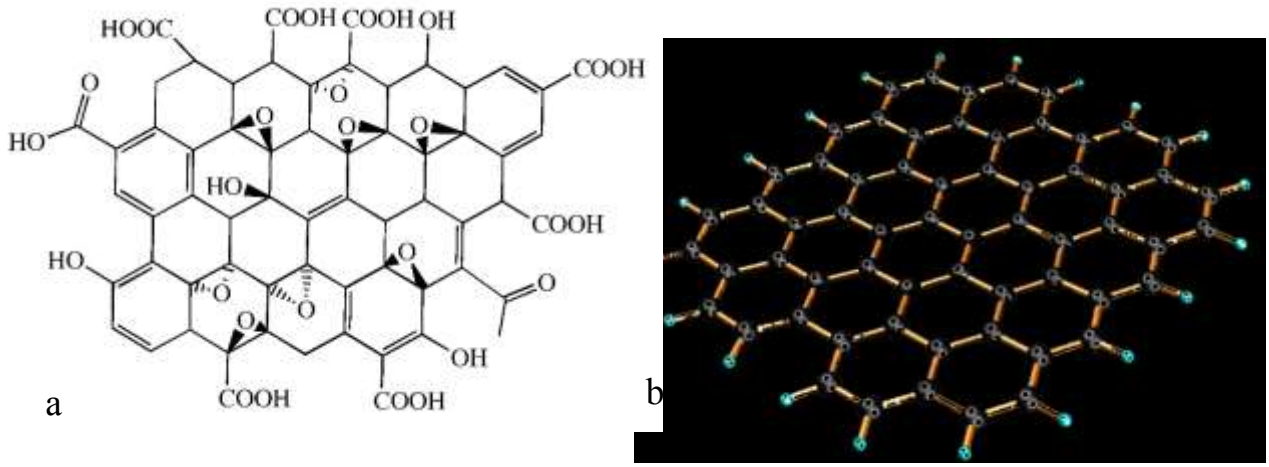

Figure 2-7: a) Chemical structure of GO showing functional groups on the surface b) molecular structure of GO showing honey-comb structure (Gao, Li et al. [50])

2.7 Iron/copper nanoparticle on support

This research focuses on ex-situ deposition of copper/iron nanoalloy on GO. Previous researches mostly focused on the in-situ deposition of Fe/Cu NPs on a support with none attempting the ex-situ deposition on GO to the author's best knowledge. Han et al. [52] embedded Cu/Fe NPs within amidoximated polyacrylonitrile (PAN) for catalytic removal of Acid Orange dye. They reported that the bimetallic PAN fiber complex performed better than iron PAN complex because of synergistic effect. They also reported 0.56 to be the optimum copper to iron molar ratio for best catalytic and stability activity of the catalyst. Luo et al. [45] similarly deposited Fe/Cu on a zeolite support for removal of phenol, in this research they reported the highest catalytic activity of the the catalyst at equal weight of copper iron and as a result minimum size and higher iron-copper interaction. Interestingly the rough surface of treated zeolite provided a better interaction of bimetal and prohibiting the metal migration. Wang et al. [53, 54] supported iron/copper BNPs on a hollow mesoporous silica spheres (HMS) for Fenton degradation of orange II organic dye. They reported 90% degradation of the dye because of synergistic effect of iron copper NPs and the "cavity effect". They also reported high (78.9%) catalytic activity after 5 consecutive runs. In similar research Wang, et al. researched the effect of Fe/Cu ratio on the catalytic performance. The results showed that the catalytic oxidation depended heavily on the Fe/Cu ratio and reported 1:3 as the optimum Fe/Cu mass ratio. They reported that the synergistic effect of iron/copper BNPs are the result of combination of iron/copper species which can accelerate redox cycles of Fe^{3+}/Fe^{2+} and Cu^{2+}/Cu^{+} [53, 54]. Table 2-3 summarizes the reported synergistic effect between iron and copper on bimetallic supported nanocomposites.

Table 2-3: Fe/Cu BNPs on support and reported synergistic effects

Nanomaterial	Support	Contaminant	Report	Reference
Fe/Cu	PAN	Organic dye	Creation of defects, novel active sites and facile redox interplay between copper and iron redox couples. Addition of certain metals to catalyst	[52]

			may stabilise the activity for the oxidation of organic pollutants in comparison with monometallic catalyst.	
Fe/Cu	Zeolite	phenol	Synergistic effect between Fe and Cu by creating defects. Synergistic effect between support increases durability and selectivity	[45]
Fe/Cu	Zeolite	Cyclohexane	This synergetic effect from dinuclear salen complexes and/or the interaction of adjacent partially coordinated Cu (salen) and Fe (salen) complex molecules through the lattice oxygen of the zeolitic host.	[55]
Fe/Cu	MCM-41	phenol	The resulting materials possessed an improved catalytic activity due to the synergistic effects of two-metal redox couples	[56]
Fe/Cu	HMS	Orange II	Interfacial electron transfer in redox cycles of Fe^{3+}/Fe^{2+} and Cu^{2+}/Cu^{+} pairs. Less pH dependency, higher stability	[54]
Fe/Cu	SiO2	diethyl malonate	Characterization results revealed that interactions between Cu and Fe contributed to the improvement of diethyl malonate conversion and selectivity to 1,3-propanediol	[40]

2.8 Toxicity of engineered nanomaterials

While nanomaterials have gained a lot of interest in environmental applications, fate and transport of these nanomaterials as well their toxicity must be assessed to safely apply these

materials in the environment. Although almost all materials can be toxic in small doses it is important to determine at what concentrations these materials can be toxic or disrupt ecology.

In this study, we synthesized a nanocomposite consisting of copper, iron and Graphene Oxide. It is crucial to determine the toxicity of these nanomaterials. Karlsson et al. [57] investigated different nanomaterials and their toxicity and ability to cause DNA damage and oxidative stress. In this study copper oxide (CuO) were the most toxic and iron oxide particles (Fe_3O_4, Fe_2O_3) showed no toxicity. Griffity et al [58] also studied different metals in both nanoparticle and soluble salts and their results showed toxicity of nanocopper for concentrations as low as 40 to 60 $\mu g\ L^{-1}$. However, in this study, nanocomposites are easily magnetically separable and dissolved concentrations of iron and copper leached to the environment are the major environmental concern.

Copper is an essential nutrient at low concentrations but toxic to aquatic organisms at higher concentrations. Copper can cause mortality and adverse effect on growth, reproduction and alteration of brain functions in aquatic organisms. Environmental protection agency (EPA) has put the criteria for copper at marine and estuaries at 2.0 $\mu g\ L^{-1}$ for acute effect and 1.3 $\mu g\ L^{-1}$ for chronic effect. The drinking water regulation for copper is 1.3 ppm according to EPA and 1 ppm according to government of Canada. Iron has proven to be less toxic and EPA criteria for iron in freshwater systems is 1 ppm [59].

Lingling Ou et al. [60] investigated toxicity of Graphene family nanomaterials in vivo and in vitro. They hypothesized that small size, high surface area and surface charge of GO may pose genotoxic properties and cause DNA damage. They reported mutagenesis in mice after intravenous injection of 20 $mg\ kg^{-1}$ in mice. They reported that DNA damage may initiate cancer or impact fertility. They also reported that GO could not interact directly with intestinal tract when ingested and therefore does not absorb to epithelial cell. Lalwani et al. [61] reviewed the toxicity of graphene based nanomaterials and the environmental impact. They reported biodegradability of GO after 5 h by 50%. None of these reports exclusively cite environmental impact of GO and recommended concentration in the environment but recommend further studies and highlight the importance of assessing long-term impact of presence of GO in the

environment. However, in this study, GO is magnetically separable and recoverable, pointing out another advantage of functionalizing GO with magnetic particles.

Chapter 3: Materials and Methods

3.1 Chemicals

Ferrous sulfate ($FeSO_4.7H_2O$), cupric sulfate ($CuSO_4.5H_2O$), nitric acid (HNO_3), hydrochloric acid (HCl), acetone (C_3H_6O) were purchased from Fisher Scientific, Canada and sodium borohydride (NaBH4,98%) and Tetracycline($C_{22}H_{24}N_2O_8$) were obtained from Sigma Canada. All chemicals were used as received. Deionized (DI) water (Milli-Q water purification system, Millipore, Bedford, MA, USA) was used as the solvent for preparing all solutions. Single layer Graphene Oxide (SLGO) was obtained from cheap tubes. Acetonitrile, methanol, isopropanol was HPLC grade. Formic acid was sequencing grade and HCl and NaOH were analytical grade and were provided by Fisher, (USA). All antibiotic stock solutions and samples were kept in the refrigerator at 4°C and sealed until use.

3.2 Synthesis and preparation of materials

3.2.1 Iron nanoparticles

The synthesis of nZVI used in the experiments was done according to the protocol by Jamei et al. [62].They demonstrated that the delivery rate is an essential factor in determining the nZVI particle size. nZVI was synthesized in a 1 L flask reactor with constant Nitrogen purging. The solution was stirred vigorously at 250 rpm. For the reduction in ferric ions to nZVI, a burette was used to deliver 100 mL of 0.4 M of borohydride solution into 500 mL of 0.08 M $FeSO_4 \cdot 7H_2O$ solution with the delivery rate of 10 ml min^{-1}. The reaction was left under stirring for an additional 20 minutes to complete hydrogen formation. The reduction reaction can be described as follows:

$$4\mathrm{Fe}^{+2}_{(aq)} + \mathrm{BH}^{-}_{4(\mathrm{aq})} + 3\,H_2\mathrm{O} \rightarrow 4\mathrm{Fe}^{0}_{(s)}\mathrm{B(OH)4(aq)} + \mathrm{B(OH)}_{4(\mathrm{aq})} + 7H^{+}_{(\mathrm{aq})} \quad (1)$$

The resulting black nZVI precipitate was collected by a magnet. The collected particles were then washed 3 times with ethanol, dried, and stored in freezer.

3.2.2 Co-assembly of Iron and Graphene oxide (Fe-GO)

The GO/nZVI composite was prepared by mixing nZVI nanoparticles with highly dispersive GO sheets in ultrapure water. Briefly, 0.05 g of nZVI was added in 10 mL of ultrapure water at room temperature and followed by 15 min ultrasonication for complete dispersion. Then a required amount of GO stock solution was added to the nZVI suspension and was vortexed for 30 s. Then the final precipitate was separated by a magnet and used freshly.

3.2.3 Iron-Copper bimetallic nanoparticle (Fe/Cu)

Synthesis of Fe–Cu bimetallic nanoparticles was carried out using a method by Morales-Luckie et al. [63] . Water was purged with nitrogen gas for 2 hours prior to the experiment. 500 ml of 5mM $FeSO_4 \cdot 7H_2O$ and 500 ml of 5 mM $CuSO_4 \cdot 5H_2O$ aqueous solutions were prepared using deionized water and mixed at 250 rpm for 20 minutes. pH was adjusted to 7.0 using 1N and 0.1 N NaOH solution. According to Morales-Luckie et al., pH plays an important part in the final composition of the nanomaterial. 100 ml of 10 mM aqueous solution of $NaBH_4$ were added drop wise with the delivery rate of 10 ml/min [63]. The reaction follows:

$$4Fe^{+2}_{(aq)} + 4Cu^{+2}_{(aq)} + 3BH^{-}_{4(aq)} + 12\,H_2O \rightarrow 4Fe^{0}Cu^{0}_{(s)} + B(OH)_{4(aq)} + 24H^{+}_{(aq)} \qquad (2)$$

The fine black precipitate of bimetallic nanoparticles was separated using a magnet. The collected particles were then washed 3 times with ethanol, dried, and stored in a freezer.

To prepare bimetallic nanoparticles with different copper to iron ratios, total concentration of iron and copper was kept at 10 mM. Iron and copper concentrations are shown in Table 3-1.

Table 3-1: Copper Iron nanoalloy synthesis with different Iron to Copper ratio

Nanomaterial ID	Iron salt concentration (mM)	Copper salt concentration (mM)	Total metal salt concentration (mM)	Sodium borohydrate concentration (mM)
F1C1	5	5	10	10
F3C1	7.5	2.5	10	10
F1C3	2.5	7.5	10	10

3.2.4 Co-assembly of Iron-Copper bimetallic nanoparticle and Graphene Oxide (nZVI/Cu-GO)

The co-assembly deposition bimetallic with graphene oxide followed the same protocol of GO-nZVI. 0.05 g of nZVI was added in 10 mL of ultrapure water at room temperature and followed by 15 min of ultrasonication for complete dispersion. Then a demanded amount of 2.5 mg of GO stock solution was added to the nZVI/Cu suspension and was vortexed for 30 s. Then the final precipitate was separated by a magnet and used freshly.

3.3 Characterization

Microstructural investigation was carried out by transmission electron microscopy (TEM, FEI Tecnai G^2 F20 200 kV Cryo-STEM), the microscope was equipped with a Gatan Ultrascan 4000 4k x 4k CCD Camera System and energy dispersive X-ray (EDS, EDAX Octane T Ultra W /Apollo XLT2 SDD and TEAM EDS Analysis System). Field emission scanning electron microscope (FESEM) images were obtained using FEI Quanta 450. The XRD patterns of the composite were obtained using X-ray diffraction by Bruker D8 Advance diffractometer operating at 40KV and 40 mM using filtered Cu Kα radiation (λ=1.5418 Å). The specific surface area was determined using Brunauer–Emmett–Teller (BET, Quantochrome Instruments autosorb-1 analyzer). Zeta potential of Fe/Cu nanoparticles were measured using Zeta Potential/Particle Size Analyzer (BrookHaven Instrument Corp., ZetaPlus / Bl-PALS, Holtsville, NY). Leaching of metal into the solution was anaylsed by Inductively Coupled Plasma-Mass spectroscopy (ICP-MS, Agilent 7500ce).

3.4 Experimental setup

3.4.1 Performance evaluation

The batch experiments for evaluating the performance of nanomaterial for removing TC was carried out in an 80 ml flask with a total solution volume of 50 ml. After adding 12.5 mg of the adsorbent, the solution was sonicated at 50% amplitude for 3 minutes in (Brandon Digital Sonifier). The solution was then placed on a rotary shaker (Innova 2000) at 150 rpm and room temperature. 3 ml of sample was periodically withdrawn, then the supernatant was filtrated through 0.2µm syringe filter and transferred to a 3 ml quartz cuvette (Agilent) and analyzed by UV-Vis spectrophotometry (Agilent Cary 8454) to determine the remaining concentration of TC. Every flask was covered by aluminum foil to avoid light exposure. A replica sample of 100 ppm TC was also covered and placed on the rotary shaker as a control. TC stock solution was covered and stored in the refrigerator prior to each experiment. Reaction parameters such as reaction time, solution pH, initial concentration of TC and adsorbent dosage that affect the performance of the adsorbent were evaluated. 0.1 M NaOH, 1M and 0.1 M HCl and 1 M HCl solutions were used for pH adjustment. All experiments were carried out 3 times and the average value of the results are presented. A control beaker containing TC solution was covered with aluminum foil and placed on a rotary shaker during the performance evaluation.

To determine the accuracy of results, limit of detection and limit of quantifications were calculated prior to data analysis. According to Agilent handbook, limit of detection (LOD) is the lowest concentration of analyte that is detectable at the most sensitive instrument settings. The detection limit is reached when the signal from the analyte is equal to three times the noise in the measurement. Limit of quantification (LOQ) is the lowest concentration of analyte that can be determined with acceptable precision and accuracy. Linearity is also an important factor, which is the ability of the method to produce test results that are proportional, either directly or by a mathematical transformation, to the concentration of analyte in samples within a given range for UV-Visible LOD and LOQ were calculated using method of detection limit (MDL).

$$LOD = 3S_b/m \quad (4)$$

$$LOQ = 10S_b/m \quad (5)$$

where S_b is average standard deviation of the intercept and m is the average slope of three measurements of the standards. Calibration curve was drawn using a blank and tetracycline concentration ranging from 0.5 to 100 ppm. Limit of detection for Cary 8454 using Quartz cuvette for tetracycline was calculated as follow:

Table 3-2: LOD and LOQ for TC peaks in UV-Vis

Wavelength	LOD	LOQ
260	0.22	0.73
360	0.53	1.76

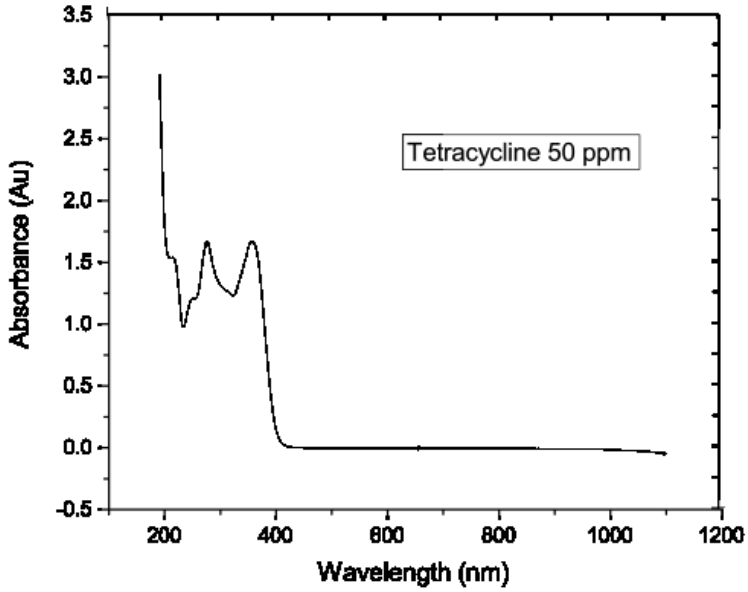

Figure 3-1: Tetracycline UV-Vis spectrum showing two distinct peak at 260 nm and 360 nm 50 ppm

As can be seen in Table 3-2, limit of detection was lower for λ_1: 360 nm, therefore 360 nm calibration was chosen for UV-VIS analysis. Performance data is presented as removal efficiency and denoted as (C/C_0).

3.4.2 LC-ESI-MS Analysis

Identification of TC products was achieved by a LC-ESI-MS (Shimadzu LC-20 AD) with ZORBAX C8 column 2.1 mm × 150 mm) with 5 μm diameter packing using the mass detector and seven level of the calibration curve. The injection volume was 100 μL. Ultrapure water (A) and methanol containing 0.1% formic acid (v/v) (B) were used as mobile phases. Gradient elution was as follows: The initial 5% B was increased to 15% within 6 min; a further 25% B was increased 40% in 6 min. Finally, the gradient was returned to the initial conditions of 5% B for 13 min. The flow rate was 0.3 mL min^{-1} with the column temperature of 40° C.

3.4.3 Durability and stability performance

To investigate the durability and reusability of the synthesized nanocomposite two separate tests were performed. The stability of nanocomposite was tested in continuous operation of 5 cycles. The reaction was performed continuously without reclaiming the nanocomposite throughout the stability test. Batch experiments were carried out in a 200 ml flask and at the beginning of each cycle a known concentration of TC stock solution was added to the reaction mixture for keeping the initial concentration constant. For this method, the initial TC concentration of 20 mg L^{-1} was chosen since low solubility of TC in water did not permit continuous operation at 100 mg L^{-1}. Similarly, for this comparison studies, dosage of the nanocomposite was reduced by to half of the optimum dosage. Reaction was carried out at room temperature without adjusting the initial pH (pH 6.5). Sampling was carried out periodically and the residual concentration of TC was measured using a UV-Vis spectrophotometer (Agilent Cary 8454).

In another attempt to determine the stability of synthesized nanocomposite, leaching of iron and copper metals from the nanocomposite was quantified by measuring the metal ion concentration after each batch experiment with ICP-MS analysis. Since most wastewater is in the pH range of 3-7 and leaching of metal ions are more severe in acidic medium, pH was adjusted to 3 at the beginning of each experiment using 0.1 M HCl. After the batch experiment, adsorbent was separated from aqueous solution using a magnet. Supernatant was filtered with 0.22 um PTFE syringe filter and the sample was diluted 100 times using 1% v/v nitric acid. After dilution, samples were analyzed using Inductively Coupled Plasma-Optical Emission spectroscopy (ICP-MS Agilent 7500ce). Samples were kept in the fridge and analyzed the next day.

Chapter 4: Results and Discussion

4.1 Nanocomposite synthesis and co-assembly behavior

Iron copper nanoalloy nanoparticles were successfully synthesized using the Morales-Luckie et al. [63]method. After complete precipitation of nanoalloy, the supernatant was tested for Iron and Copper salt residual with UV-Vis but no traces of metal salts could be detected. (UV-Vis absorbance for $Fe(SO)_4^{2-}$ =350nm and $Cu(SO)_4^{2-}$=635 nm). All precipitated nanoparticles were separated and washed using a magnet indicating that iron was integrated in the structure of all nanoparticles. The supernatant of the magnet separation was then placed in the centrifuge at 12,000 rpm for 3 minutes. An insignificant amount of nanoparticles could be collected confirming that nanoparticles contain both iron and copper.

The nanoparticle synthesis was condition dependent. Higher or lower pH could result in unsuccessful formation of nanoalloys. Morales-Luckie et al [62] investigated the effect of pH on the final weight percentage of nanoparticles and reported that for the pH under 7, higher copper content nanoparticles were formed, while at pH 7.0 an almost 50/50 iron to copper ratio NPs were formed. This phenomenon can be explained by the fact that i) reduction of Fe^{2+} occurs more easily for pH near 7 while this pH value is significantly lower for Cu^{2+}; ii) normal oxidation potential is a factor since more positive oxidation potential results in better reduction in non-controlled pH processes. According to Yedra et al. (2003) oxidation potential for Fe is E_0=-0.44V, and for copper is E_0=0.34V [64]. Therefore, precipitation of copper is more favored at lower pH values resulting in a higher Cu content nanoalloy in acidic conditions.

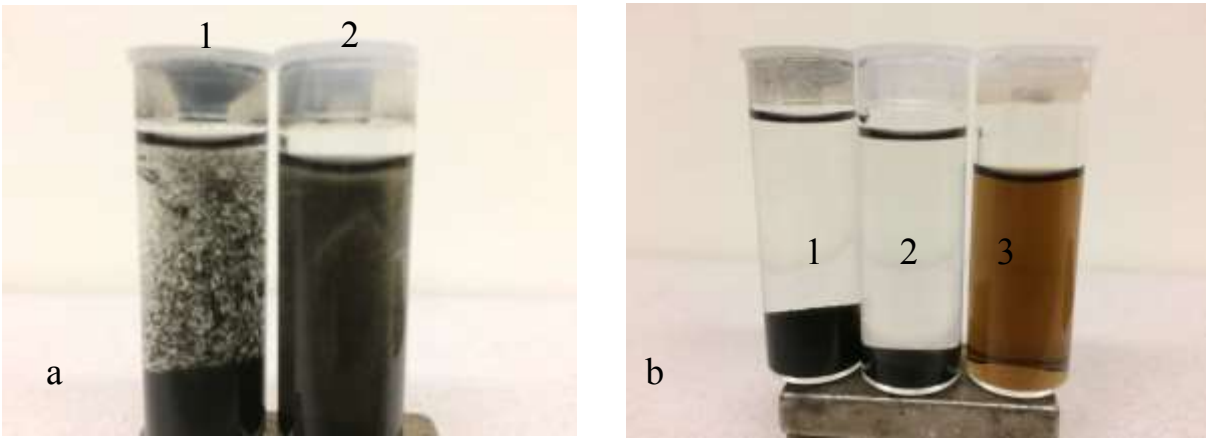

Figure 4-1 :a)1) fluffy structure of GO supported NP 2) Fe/Cu BNP suspension (b) (1 &2) volume comparison between supported and unsupported NP (3) stable GO suspension after 24 h

Synthesized nanoparticles were then added to GO stock solution (0.5 mg ml^{-1}) and vortexed for 30 seconds. GO is highly dispersive in water and can maintain homogenous brown suspension even after 48 h as can be seen in Figure 4-1. According to Konios et al. [65] who investigated dispersion behavior of GO in 18 solvents, GO can maintain a uniform suspension in water even

after two weeks. After introducing the synthesized nanoalloy to the GO stock solution, formation of nanocomposite is instantaneously visible. Nanocomposite forms a blanket with a small thin layer of clear water on top. After placing a magnet underneath the vial, the blanket compresses and forms a layer of black precipitant which possess 3-4 times volume of nanoalloy (GO volume is negligible). Nanocomposite is fluffy in texture and possessed a 3D structure. For GO loading values less than 7-10% wt, the clear supernatant does not contain any graphene oxide. On the other hand, for GO loadings higher than 10% a residual suspension of GO is visible.

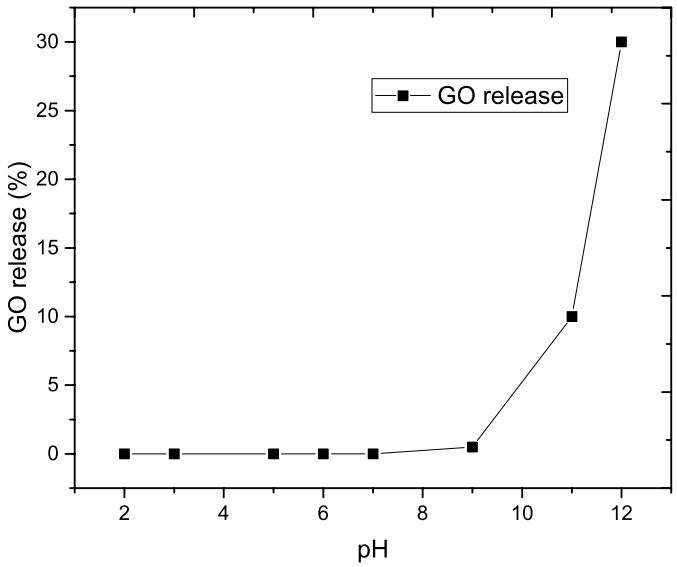

Figure 4-2: GO release test performed with dosage of 0.2 g L-1 dosage of nanocomposite and absorbance at 270 nm

To better demonstrate the reversibility of the co-assembly behavior, 10 mg of synthesized supported BNP with GO loading of 5% was dispersed in DI water. The solution of pH was adjusted with 0.1M HCl and 0.1 M NaOH. For every pH value, a sample of effluent was tested with UV-Vis to detect GO in the solution at absorbance value of 270 nm. Maximum concentration of GO was roughly estimated at 10 ppm based on the 5% GO loading, consequently, percentage of GO release was calculated using the estimated maximum concentration and released GO concentrations. As can be seen from Figure 4-2, for acidic and

neutral conditions, self-assembly is favored resulting in no detection of free GO. For pH values, higher than 9 supernatants of solution becomes brown, suggesting presence of free GO in the solution. This observation was also confirmed with UV-Vis. Although, only 30% GO release was observed in this experiment, Liu et al. [46]suggested the possibility of 73% GO release for pH values higher than 12. This behavior is reversible and the assembly takes place after lowering the pH. Figure 4-3 shows schematic presentation of assembly behavior of Cu/Fe BNPs and GO, showing the possibility of spent nanoparticle reclamation and GO regeneration with a pH sensitive assembly.

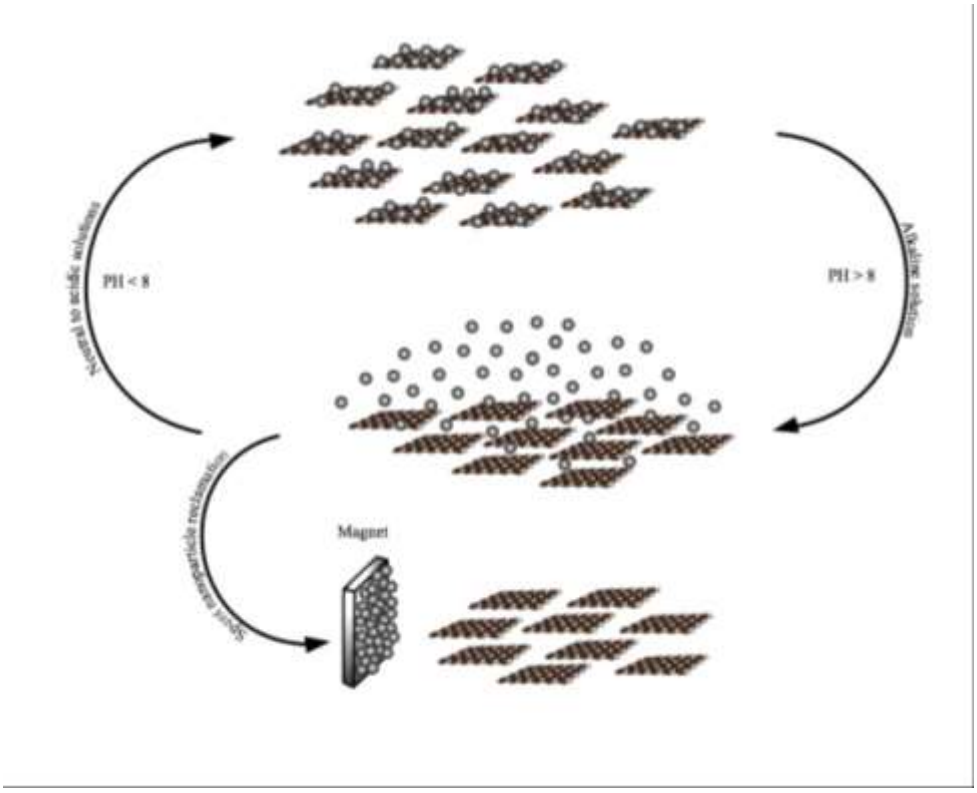

Figure 4-3:pH-sensitive co-assembly behavior of GO and Cu/Fe BNPs, this assembly is favored for neutral and acidic conditions

The co-assembly behavior of GO and Fe/Cu can be explained by zeta potential of these two nanoparticles. Zero point of charge (ZPC) for Fe/Cu nanoparticles falls between values of 8 and 9 as seen in (See Appendix). ZPC of GO is around pH 2 according to Liu et al. [46]. At solution pH between 2 and 8-9, positive ZPC of Fe/Cu nanoparticles and negative ZPC of GO nanoparticles will lead to electrostatic attraction between two nanoparticles and therefore favoring the nanohybrids production. Jiao et al. [34] reports several benefits for *ex-situ*

deposition over i*n situ* deposition of Fe_3O_4 on GO for removing organic dyes. The ability to control the size of nanoparticles prior to anchoring to GO sheets and the ability to regenerate GO and not losing the surface area of GO with permanently anchored nanoparticles makes the ex-situ method an interesting method. Liu et al. [46] have a noteworthy approach in using this assembly behavior. *Ex-situ* prepared GO-nZVI nanoparticles were used for adsorption of TC from aqueous solution, the adsorbent was further separated by a magnet and placed in an alkaline solution for adsorbent generation. Desorbed TC was then degraded using ozonation. Therefore, this co-assembly behavior presents an interesting area of research in adsorbent regeneration and recycling.

4.2 X-ray Diffraction

XRD has been widely employed to study supported and unsupported adsorbents and catalysts to gather information on the structure, lattice spacing, grain size and crystallinity. XRD pattern of Fe/Cu and Fe/Cu-GO are displayed in Figure 4-4. XRD pattern of Fe/Cu are in good agreement with XRD pattern obtained by Morales- Luckie et al [63] for Fe/Cu nanoalloy. The diffractogram exhibits a structure of a bimetallic nanomaterial where iron atoms are presumably embedded within the copper matric. This structure is typically found in one-step synthesis of bimetallic nanomaterials. Morales-Luckie et al.[63] also reported face centered cubic(FCC) structure for this nanoalloy. The prominent peak at 35° indicates the presence of copper and iron oxide on the surface of the lattice which is consistent with value given in Joint Committee on Powder Diffraction Standards (JCPDS) diffraction data files. It means that a part of nanoalloy is covered with Fe_3O_4. Iron oxide can be formed during synthesis, drying and XRD sample preparation. For 2-Theta values lower than 30°, a high background is detected indicating amorphous behavior that can be associated with organic decomposition products or residual solvents left in the sample [66]. Moreover, a clear diffraction peak at 44.6 in Fe/Cu can be observed, which corresponds to the (110) diffraction of a Fe (indexed to JCPDS no. 06-0696) and (111) diffraction of copper (indexed to JCPDS no. 99-0034).

After combination with GO, the peak corresponding to GO (2-Theta 10.99°) is not visible but the peak at 44.9^o have increased and broadened. GO peak is not visible partly due to the small weight

percentage of GO in comparison to the metal weight fraction and partly because of Fe-Cu nanoalloys anchored on the surface of GO sheets prevented restacking of the layered structure of GO [67]. Disappearance of (001) planes of GO or any other support in XRD pattern was mentioned by other articles [34, 46, 47].The complete list of corresponding peaks are shown in Figure A-1 (see appendix).

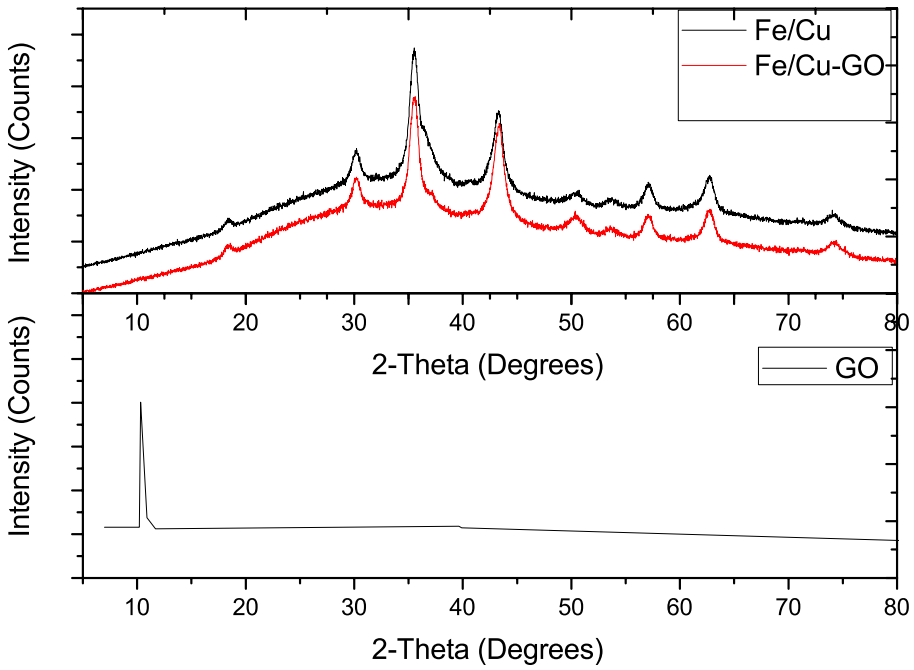

Figure 4-4: Overlaid XRD pattern for Cu/Fe and Cu/Fe-GO showing that the supported BNP does not have a peak corresponding to GO

4.3 SEM, TEM and EDS

The morphology and nanostructure of Fe/Cu nanoparticles and GO supported Fe/Cu nanoparticles were investigated using scanning electron microscopy (SEM) and transmission electron microscope(TEM). SEM images of bimetallic nanoparticles (Figure 4-5) show sphered nanoparticles which are highly clustered. This agglomeration is a result of magnetic and

electrostatic attractions. Since the boundaries of nanoparticles are not clear, the size of nanoparticles cannot be determined from SEM images. GO-supported SEM images (Figure 4-6) show an even distribution of Fe/Cu nanoparticles on the surface of GO. In fact, no individual the NPs can be observed beyond the GO sheets, suggesting a strong interaction between NPs and GO sheets. The SEM structure of nanocomposite with 15% GO loading is shown in Figure 4-9. The SEM images suggest a different structure for nanocomposite with higher GO loading in which the nanoparticles are intercalated between GO sheets.

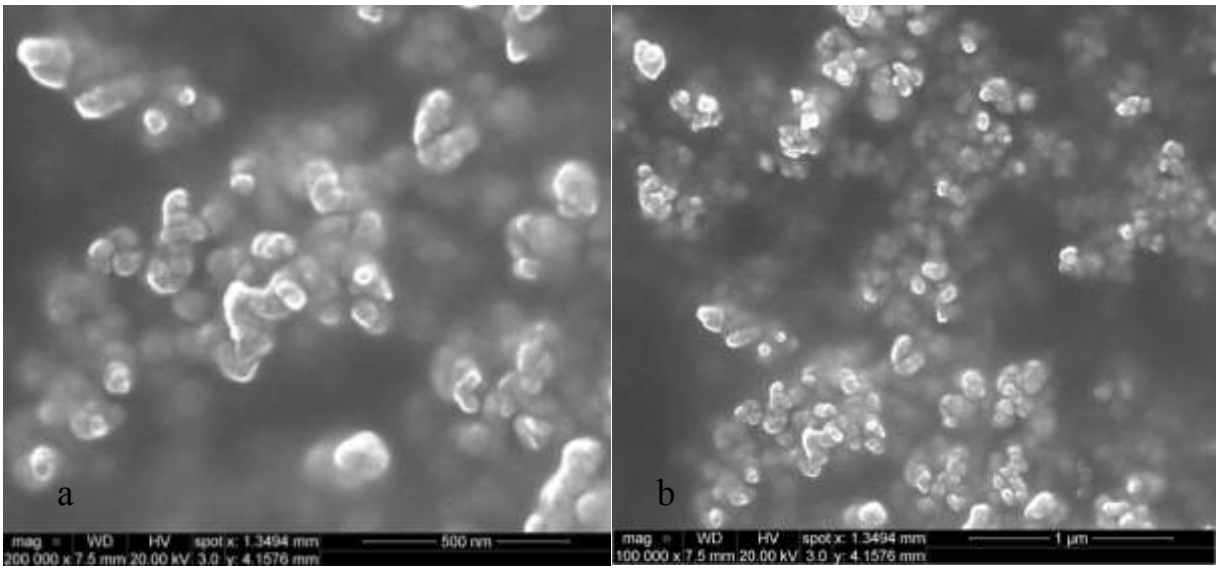

Figure 4-5:SEM images of Fe-Cu nanoparticle showing agglomerated clusters of nanoparticles a) 500 nm scale b) 1µm scale

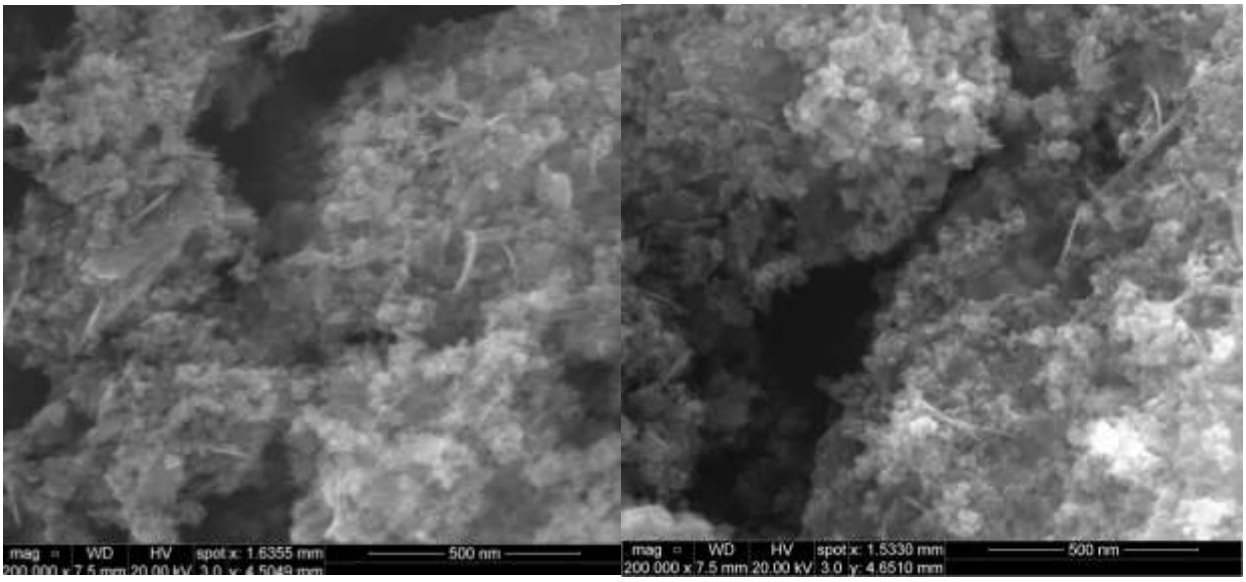

Figure 4-6: SEM Image of Fe/Cu supported on GO showing the sharp edges of GO with clustered nanoparticles depositing evenly on the surface (GO loading 5 wt%)

TEM images and EDS results for Fe/Cu NPs and GO-Fe/Cu NPs are shown in Figures 4-7 and 4-8 respectively. TEM images for FE/Cu NPs show a clear boundary for each sphere. The nanocluster and chain like formation of these NPs are also clearer in TEM images. The size of NPs ranges from 4 nm to 12 nm, with an average size of approximately 8 nm. This finding is in good agreement with the previous approximation of NP size based on BET results. The size of nanoparticles also matches those prepared by Morales Lukie et al. [63] who reported average size between 4 to 8 nm for synthesized nanoalloys. EDS results confirmed the formation of nanoalloy with elemental Fe and Cu present. Oxygen is also present suggesting partial oxidation of iron and copper.

TEM images of GO supported Fe/Cu NPs show a homogenous distribution of NPs on the surface of GO with each nanocomposite having an approximate size of 100 nm. Figure 4-8 (a) shows a partially uncovered GO for better demonstration of the monolayer anchored Fe/Cu NPs on the GO sheet and the ideal structure for lower GO loading. EDS elemental mapping also confirmed the presence of iron and copper element as well as the carbon element.

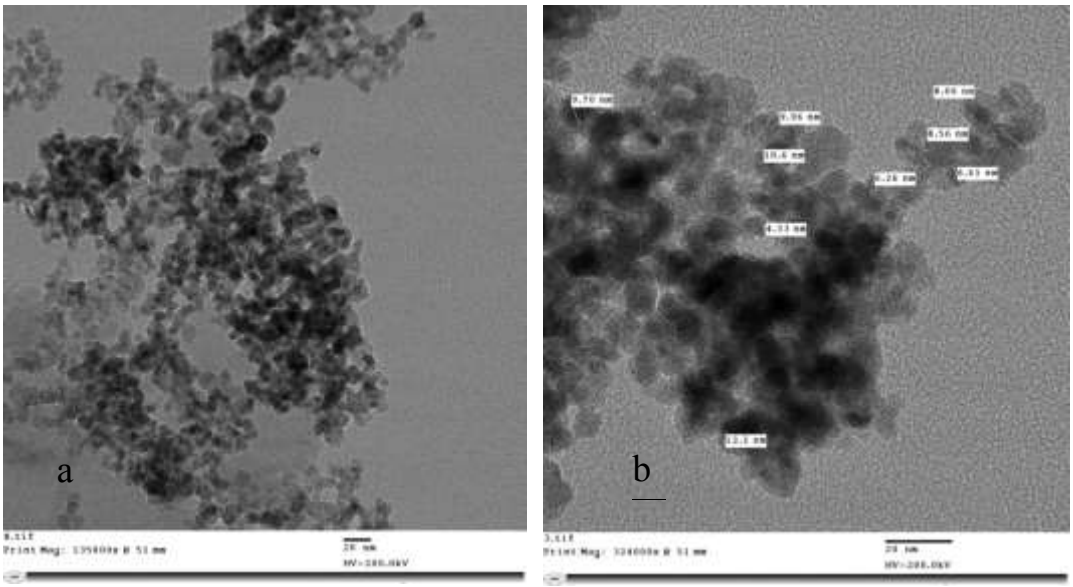

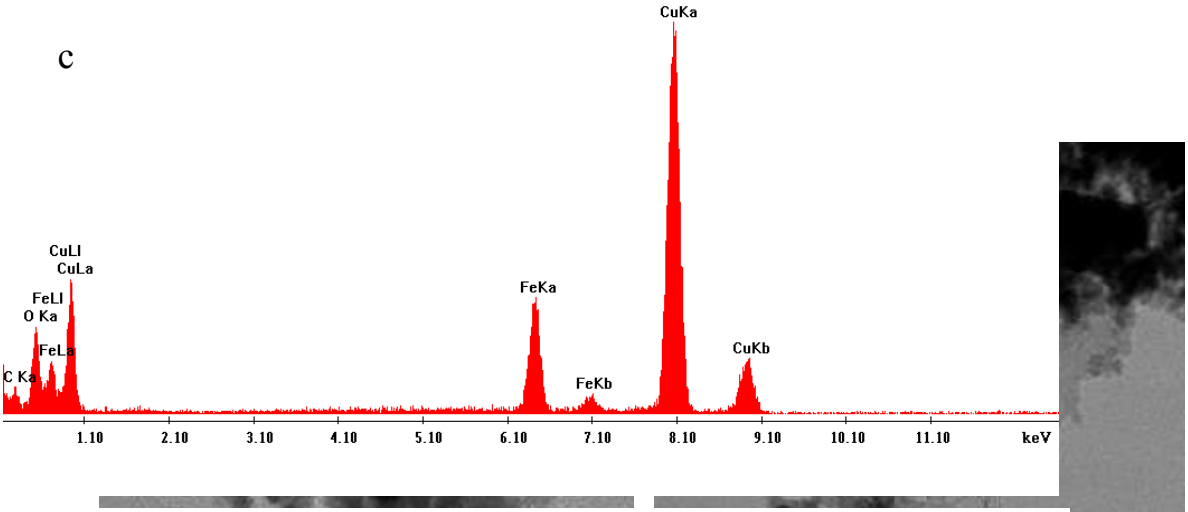

Figure 4-7: a) TEM image of Cu/Fe BNP b) TEM image of BNPs showing the approximate size of each particle C) EDS elemental mapping of nanoparticles showing the presence of iron, copper and oxygen

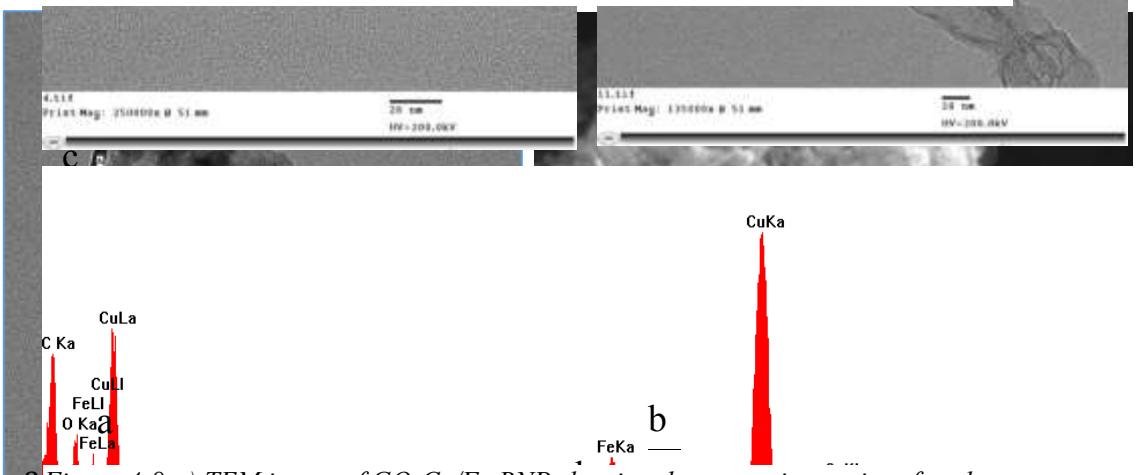

Figure 4-8:a) TEM image of GO-Cu/Fe BNP showing the approximate size of each nanocomposite b) transparent GO sheet is clearly visible and BNPs are deposited on the GO Figsupport C) EDS elemental mapping of nanoparticles showing the presence of iron, copper, loaoxygen

4.4 Surface Area (BET)

Specific surface area of the composite can be determined with the Brunauer–Emmett–Teller (BET) method. A systematic sorption and desorption of nitrogen performed by Quantochrome Instruments autosorb-1 analyzer can calculate the BET isotherm and consequently provide the fundamental information on the surface characteristics and the total surface area. Prior to characterization samples were dried at 125° C for 1 h. It is noteworthy to mention that at the end of the experiment Fe/Cu samples were reduced to a brown powder, while the GO supported nanoparticle stayed as a fine black powder.

The BET surface area for the Fe/Cu nanoparticles was 65.88 m^2 $g^{-1.}$ Aslan et al. [44] reported the BET surface value of 25 m^2 g^{-1} for synthesized ex-situ Fe/Cu bimetallic nanoparticles. Chen,H et al. [37] reported the value of 36.90 m^2 g^{-1} for PVP-nZVI nanoparticles and from this value they estimated the effective mean radius of iron particles using the following equation:

$$r = 3[\rho * S_{BET}]^{-1} \qquad (3)$$

where ρ is the density of the nanomaterial, S_{BET} is the surface area and r is the effective radius of the nanoparticle. To estimate the effective radius of nanomaterial, the density can be estimated by assuming a 1:1 Fe, Cu composition.

Where,

$\rho(Fe)$ =7870 kg m^{-3} and $\rho(Cu)$ =8940 kg m^{-3}

Average density for (1:1) Iron-Copper= 8405 kg m^{-3}

r= 3/ (8405 kg m^{-3}*1000 g kg^{-1} *65.88 m^2g^{-1}) = 5.4 nm

After deposition of nanoalloy on GO surface, BET surface area increased to 108.62 m^2 g^{-1}. This 64% increase in the surface area can be due to increase of the surface area because of GO or change in pore size of the synthesized composite. Similarly, Zubir,N.A et al. [47] reported a 58% increase in BET surface area when Fe_3O_4 NPs were deposited on GO. They also reported that by increasing GO loading from 0.5 wt% to 10 wt%, BET surface area were consistently within the

range of 115-130 m^2g^{-1}, meaning that addition of GO does not change the N_2 isotherms. Therefore, GO is not contributing significantly to the increased BET surface area. From this observation, they concluded that the increased surface area is due to changes in pore volume of GO-Fe_3O_4. They also reported that GO loading of more than 10 wt% resulted in flattening out the 3D structure of the shape and significant loss in pore volume. Therefore, it can be concluded that there are two possible structures when loading metal nanoparticles on graphene Oxide. The structure happens on small GO loading (<10%) where GO plays a marginal role in the structure and the nanoparticles anchor on the GO surface resulting in high pore volume. The second structure happens at higher GO loading, where nanoparticles are sandwiched between sheets of GO possibly leading to GO-metal stacking. Considering the high BET surface area in Fe/Cu-GO composite we can confidently say that we achieved the first desired structure. Since increased surface area of GO supported nanoparticle is a result of pore volume increase rather than size decrease, it is not accurate to estimate the particle size based on the BET surface area.

4.5 Performance evaluation

4.5.1 Influence of reaction time

To determine the optimum reaction time, batch experiments were carried out for 240 minutes and the results are shown in Figure 4-10. Under optimum conditions (pH 6.5, TC 100 mg L^{-1}, room temperature, 250 rpm) most of the contaminant was removed within 15 minutes and no peak for tetracycline could be detected after 20 minutes. However, to investigate the effect of certain parameters on removal performance, reaction time of 60 minutes was chosen as an optimum reaction time.

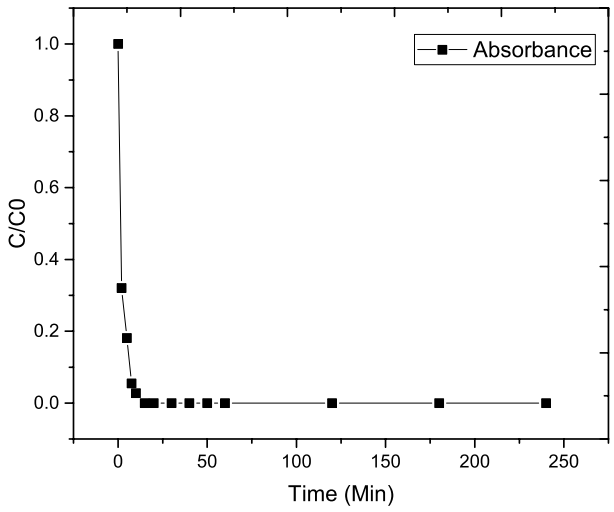

Figure 4-10: TC batch experiment at optimum condition (pH=6.5, [TC]i=100 ppm, dosage: 0.25 g L^{-1}, room temperature)

4.5.2 Removal Performance of synthesized nanomaterials

To compare the removal performance of the synthesized composite, removal performance of Fe-Cu and nZVI were evaluated at optimum conditions (initial TC 100 mg L^{-1}, pH 6.5, dosage 0.25 g L^{-1}) and the results are shown in Figure 4-11.

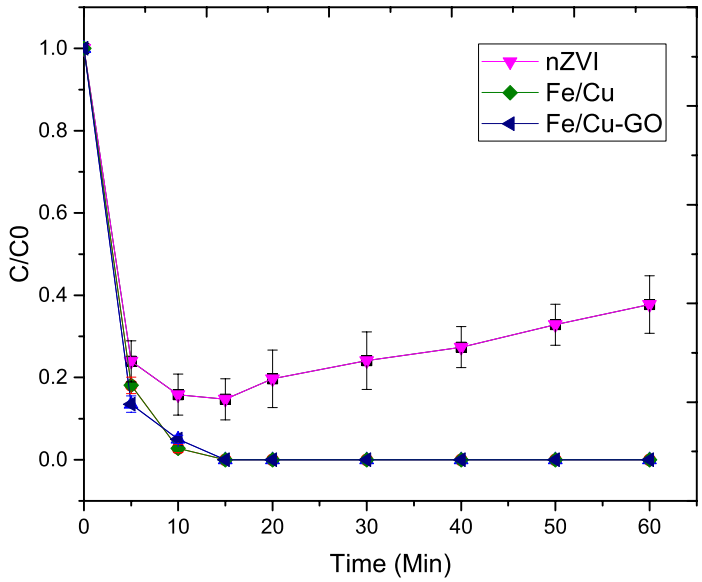

Figure 4-11: Comparison of synthesized nanomaterials performance for nZVI, Fe/Cu BNP and Fe/Cu-GO, (conditions: pH 6.5 unadjusted $[TC]_i$=100 ppm, dosage: 0.25 g L^{-1})

Hanay et al. [36] reported 100% removal of 60 ppm TC by nZVI with nZVI dosage of 0.4 gL^{-1} and 90% for dosage of 0.2 g L^{-1} at pH 6. The difference of the reported value can be attributed to the lower initial concentration of TC compared to this study.

Gao et al. [50] reported removal of TC with 400 µL of stock solution of 0.544 mg ml^{-1} GO was incubated for 24 h at 25°C. They reported a q_m of 313.480 mg g^{-1} for GO dosage of 0.18 mg ml^{-1} and TC initial concentration of 8.33 mg L^{-1} at pH 3.6. To investigate the removal TC by dispersed GO nanoparticles, two batch experiments were performed at pH 3.8 and tested periodically for 4 h. As can be seen in Figure 4-12, no removal could be detected within 4 h of reaction time.

Since residual TC concentrations or q_e values were not reported by Gao et al. [50] and all results are presented as isotherm constants results cannot be compared. However, given that GO content of composite is 2-5wt% and overall dosage of 0.01 g L^{-1} per experiment, adsorption of TC by GO can be neglected. Needless to say, presence of GO can be a great advantage when working with lower concentrations of TC (closer to concentrations of TC in wastewater and environment). Liu et al.[46] reported removal of TC by ex-situ prepared GO-nZVI for removal of highly diluted

TC. Similar observation was reported by Lin et al. [68] in which magnetic particle(MP) modified GO was used to remove TC from synthetic waste water with q_m of 39.1 at optimum conditions (TC 50 mg L^{-1}, 0.2 g L^{-1} GO-MP ,pH various). Ghadim et al. [69] reported similar TC adsorption capacity of 323 mg g^{-1} for GO with almost 15% removal of 100 ppm TC at optimum pH condition for overnight incubation of TC.

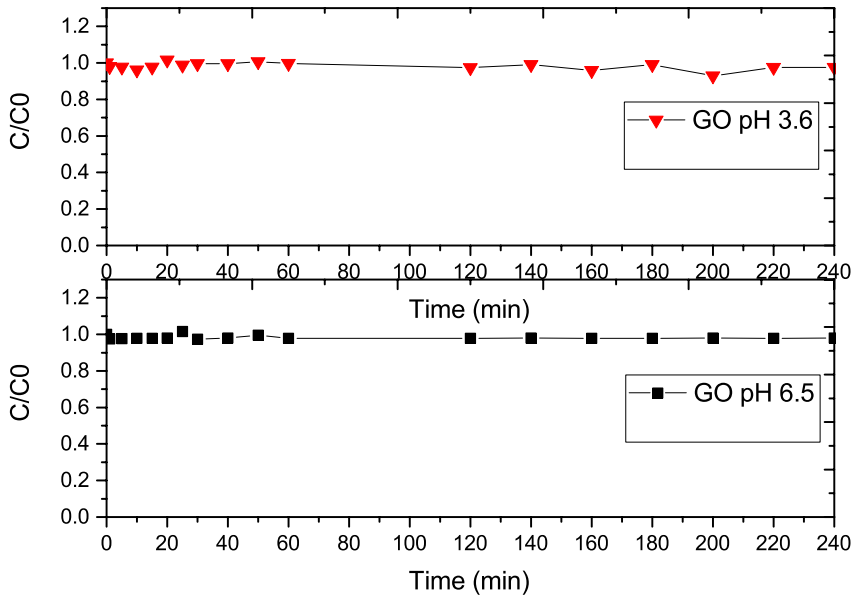

Figure 4-12: TC removal by GO for pH 3.6 and 6.5 showing almost no significant TC removal within 4 h (conditions: $[TC]_i$=100 ppm, dosage GO:0.2 g L^{-1})

Chen et al. [37] reported removal efficiency of 80% for bare nZVI for initial concentration of TC 100.0 mg L^{-1}; temperature 25 °C; pH, 6.5 and bare nZVI dosage of 0.1 g L^{-1}. Hanay et al. [36] reported 98-99% removal of TC for initial concentration of TC 60.0 mg L^{-1}; temperature 25 °C; pH 5 and pH 6; bare nZVI dosage of 0.4 g L^{-1} and contact time of 2 h. Increase of the TC concentration after 30 min can be the result of partial desorption of TC from nZVI surface because of pH increase. It was observed that the solution pH increases dramatically when nZVI is added to the solution.

Both Fe/Cu and Fe/Cu-GO showed a good performance achieving almost complete removal

within the first 15 min at optimum reaction conditions. UV-Vis results showed an almost complete removal and this finding was confirmed by LC-MS analysis of the effluent presented in Figure A-4 (see Appendix). Enhanced removal performance of Fe/Cu nanoparticles in comparison with iron nanoparticles can be explained by the synergistic effect of Fe/Cu nanoparticles. Han et al. [52]linked the synergistic effect to possible creation of defects and therefore novel active sites as well as redox interplay between copper and iron redox couples. To elaborate more, degradation of organic compounds by iron NPs are done either by direct reduction of pollutants by accepting electron generated by iron NPs or indirect reduction by hydrogen production. In copper iron bimetallic systems, high reduction potential 0.777 V between Cu and Fe can improve the electron emission rate of Fe. Moreover, addition of copper and certain metals can stabilize the activity of oxidation of organic pollutants in comparison to pristine iron nanoparticles. [45, 52, 55, 56, 70, 71]. However, to take advantage of these effects the perfect copper to iron ratio should be determined. Equal molar ratios of iron salt to copper salt showed the best removal performance and the least leaching. The 1:1 Fe to Cu ratio was used for further studies (See Table A-2 in Appendix).

Although GO supported Fe/Cu does not show an increased removal towards TC in the first cycle, the effect of the support magnifies itself further on during stability experiments. Huang et al.[72] reported that adsorption of TC to zeolite has increased from 34% to 95% in the presence of Cu(II), Wang et al. [73] also reported the co-adsorption of Cu-TC complex into Montmorillonite. Similarly, Guler et al. [22] reported a slight increase in TC adsorption into pumice stone claiming that Cu^{2+} plays a role bridging TC and copper. This phenomenon has been mentioned in many articles and it is worthy of mentioning that although copper leaching is insignificant (<1 ppm) it could possibly bridge with TC and co-adsorb into GO. Although this is just a theory, further comprehensive research can be done to confirm or reject this hypothesis [72].

Adsorption isotherms are used to investigate the relationship between the amount of contaminant adsorbed and the residual contaminant concentration remaining in the solution. Among these isotherms, Langmuir and Freundlich isotherm equations are most frequently used). The Langmuir model assumed monolayer adsorption, referring to homogenous adsorption, which

each molecules possesses constant enthalpies and sorption activation energy (all sites possess equal affinity for the adsorbate)[74]. The Langmuir model follow:

$$q_e = \frac{q_m \mathrm{K}_b C_e}{1+\mathrm{K}_b C_e} \qquad (6)$$

And can also be written in the linear form:

$$\frac{C_e}{q_e} = \frac{1}{q_m \mathrm{K}_b} + \frac{1}{q_m} C_e \qquad (7)$$

where q_m is the maximum adsorption capacity of the TC (mg g^{-1}), *Ce* is the liquid phase equilibrium concentration of TC (mg L^{-1}), q_e is the amount of TC adsorbed (mg g^{-1}), and K_b is the constant related to the energy or net enthalpy of adsorption or in other words affinity of the binding sites [74].

Freundlich model describing the non-ideal and reversible adsorption, is not restricted to the formation of monolayer. This empirical model can be applied to multilayer the adsorption, with non-uniform distribution of adsorption affinities over the heterogeneous surface. The Freundlich equation follows:

$$q_e = K_F C_e^{\frac{1}{n}} \qquad (8)$$

And can also be written in the linear form:

$$\log q_e = \log K_F + \frac{1}{n} \log C_e \qquad (9)$$

where q_e (mg g^{-1}), is the amount of TC adsorbed, C_e (mg L^{-1}) is the equilibrium concentration of TC in solution, K_F (mg g^{-1}) can be taken as a relative indicator of adsorption capacity, and *1/n* is indicative of energy or intensity of the reaction ranges between 0 and 1. Adsorption is becoming more heterogeneous as the amount of *1/n* value gets closer to zero, whereas a value below unity implies a chemisorption process [74].

Based on adsorption parameters obtained by fitting both Freundlich and Langmuir, q_m=302.5

mg g^{-1} and K_f=201.9 mg g^{-1}. The Freundlich fit better to experimental data which can be explained by the heterogeneous nature of the nanocomposite and partial simultaneous degradation. The Freundlich constant n is 6 and n>1 represents favorable adsorption conditions. Maximum adsorption capacity obtained by Langmuir is 302 mg g^{-1} exhibiting that the adsorption capacity is almost 3 times the surface area. Adsorption capacity of this study can be compared to other studies summarized in Table 4-2.

.

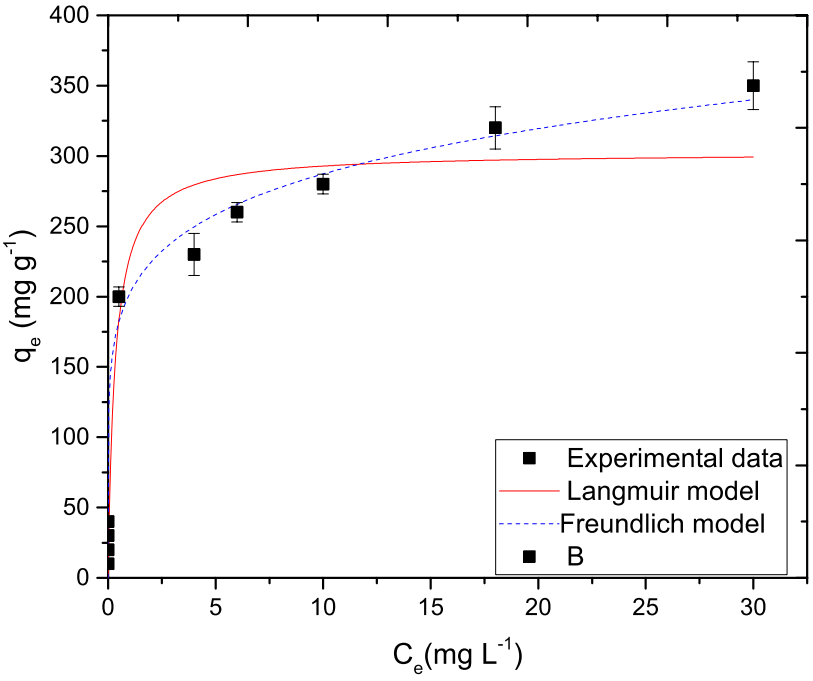

Figure 4-13: Adsorption isotherms for Tetracycline removal at optimum condition with different initial concentrations and fitted Langmuir and Freundlich model

Table 4-1: The comparison of adsorption capacity of different adsorbents for TC at optimum conditions

Adsorbent	Adsorption capacity (mg g^{-1})	Reference
Microscale ZVI	13.59	Hanay et al. (2014) [75]

Magnetic molecularly imprinted nanoparticles	14.31	Dai et al. (2012)[76]
Chitosan	20.74	Oladoja et al. [77]
GO-MPs	39.1	Lin et al. [68]
Ferric-activated SBA	54.53	Yang et al. [78]
Fe/Cu	133.3	Aslan et al. [44]
nZVI	158.73	Hanay et al. [36]
Magnetic hypercrosslinked resin	214.85	Zhang et al. [79]
Magnetic microsphere	277.49	Zhou et al.[80]
Fe/Cu-GO	302.5	This study
GO	313	Gao et al.[50]
Fe_3O_4 deposited polyacrylonitrile nanofibers	315.31	Liu et al. [81]
Fe_3O_4-G	336	Zhang et al. [82]
Activated Carbon	375.4	Rivera-Utrilla et al. [83]

Table 4-2: Adsorption parameters based on Langmuir and Freundlich model

Adsorption Isotherm model	Equation	Parameters	R^2
Langmuir	$q_e = \frac{q_m K_b C_e}{1 + K_b C_e}$	q_m=302.5 K_b=3	0.933
Freundlich	$q_e = K_F C_e^{\frac{1}{n}}$	K_f=201.9 n=6.52	0.972

4.5.3 Influence of adsorbent dosage

To determine the optimum dosage of nanocomposite for removal of 100 mg L^{-1} TC, the same batch experiment (room temperature, pH 6.5 unadjusted) was performed for different nanoparticle dosages ranging from 0.05 to 0.25 g L^{-1}. These results demonstrated that the removal profile of tetracycline increased significantly as a function of dosage from 0.05 to 0.25 g L^{-1}.

Such enhancement in removal can be attributed to the increased number of available active sites on the surface of nanocomposite. Further increasing the dosage did not increase the removal profile significantly. Therefore, a dosage of 0.25 g L^{-1} was chosen as an optimum dose for all subsequent experiments.

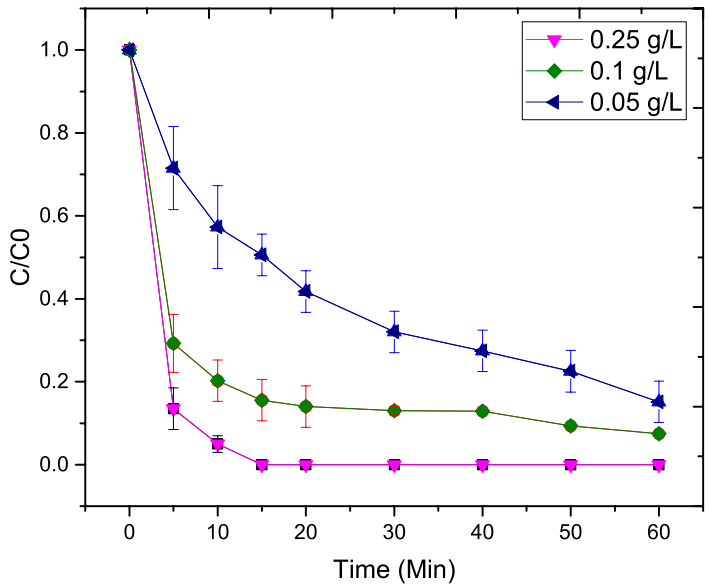

Figure 4-14: Effect of adsorbent dosage on TC removal (pH=6.5 unadjusted conditions: [TC]i=100 ppm, dosage= 0.05,0.1 and 0.25 g L-1)

4.5.4 Influence of solution pH

The pH value plays an important role in catalytic and adsorption processes. pH value can affect the mechanism and effectiveness of treatment by influencing i) degree of ionization of pollutants (pKa values for TC are 3.3, 7.7, 9.7 [1]); ii) the surface charge of the adsorbent; iii)disassociation

of functional groups on the active sites of the adsorbent and iv) bond between the support and the anchored nanomaterial [44, 47, 75].Thus, it is important to study the effect of pH on removal of TC by the synthesized composite. It can be deducted from the results that removal of TC with Fe/Cu-GO is not very pH dependent with the best removal at pH 5 to 7. Typical waste water has the pH carrying from 3 to 7, therefore, this range was chosen for pH studies. Aslan et al. [44] used a broader range of pH from 2-9 and reported an almost complete removal of TC for pH values 3 to 9. Chen et al.[37] reported pH 6.5 as an ideal pH for removing TC with PVP-nZVI [37, 46, 84].

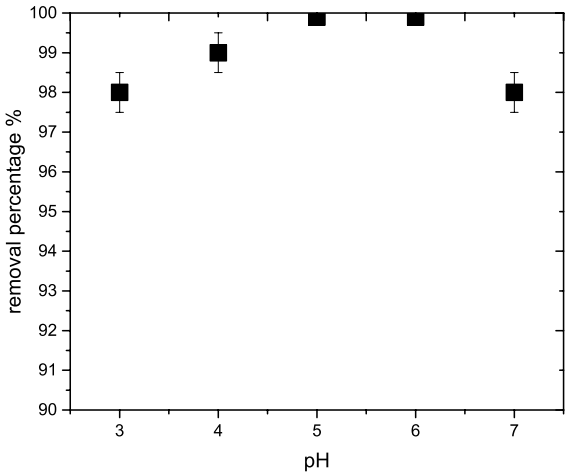

Figure 4-15: Effect of pH on removal efficiency of Fe/Cu-GO (condition: $[TC]_i$=100 ppm, dosage= 0.25 g L^{-1})

TC removal efficiency's dependence on pH can be explained by the complex chemistry of TC. As mentioned before TC has 3 pKa values. The cationic form is present for pH<3.3, and from pH 3.3 to pH 7.7 the percentage of neutral TC increases reaching 98% at pH 5, therefore increasing the affinity towards GO supported NPs [44] . Liu et al.[46] hypothesized that the slight decrease of removal efficiency for pH values higher than 7 could be the result of slight increase in repulsive forces between the nanoparticles and therefore inhibiting the adsorption of TC into the NPs.

The final pH of the reaction is reported in Table 4-4. All pH values were rounded up or down to the closest 0.05 value since the pH meter results can fluctuate and the pH meter was calibrated several times during these experiments. The increase in final pH for pH values lower than 7 is the result of the anaerobic (Eq. 10) or aerobic (Eq. 11) oxidization of Fe^0 according to the reactions below:

$$Fe^0{}_{(s)} + 2\,H_2O \rightarrow Fe^{+2}_{(aq)} + 2OH^-_{(aq)} + H_{2(g)} \qquad (10)$$

$$2Fe^0{}_{(s)} + 4\,H^+_{(aq)} + O_{2(aq)} \rightarrow 2Fe^{+2}_{(aq)} + 2\,H_2O \qquad (11)$$

Table 4-3: Influence of pH on removal efficiency and final pH

Initial pH	Final pH	Removal %
3.0	4.3	97
4.0	5.5	98
5.0	6.4	~100
6.0	6.8	~100
7.0	6.5	~100
8.0	7.5	97

4.5.5 Durability and stability performance

Stability is a crucial factor for assessing the applicability of an adsorbent and catalyst. The ability to perform for consecutive runs depend on surface passivation of NPs and metal leaching. To assess the stability of synthesized nanohybrids, 5 consecutive batch experiments were performed without adsorbent reclamation. In each batch experiment, the desired stock solution was added to keep the initial concentration at approximately 20 mg L^{-1}. The experiment was carried out 3 times and the average of 3 results are shown in Figure 4-16.

Results show that GO-Fe/Cu nanocomposite exhibited excellent stability comparing to Fe/Cu BNPs over 5 cycles, without losing activity for removal of TC. Conversely, this removal efficiency was found to decline quickly for iron/copper BNPs.

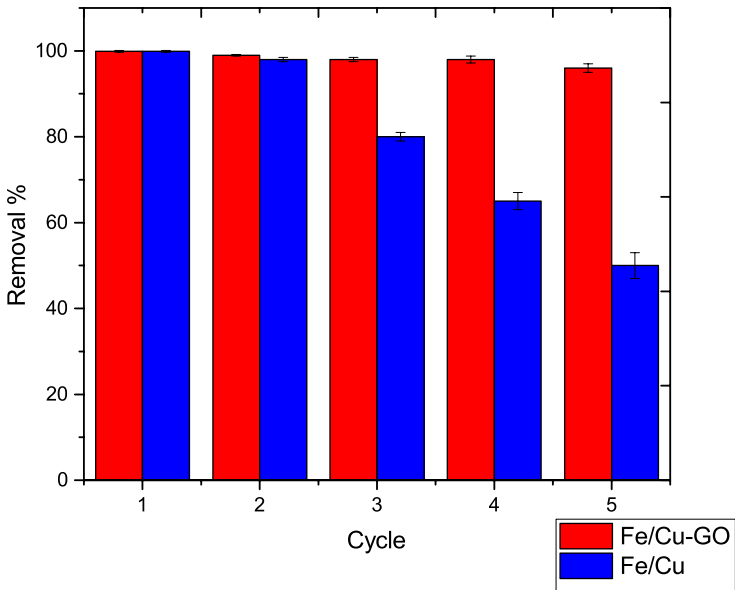

Figure 4-16: Stability comparison of Fe/Cu NPs and GO supported Fe/Cu NPs. (conditions: pH 6.5 unadjusted [TC]i=20 ppm, dosage= 0.13 g L-1), GO supported BNP showed significant stability in comparison to unsupported BNP

The mechanism associated with the synergistic effect between the interfacial interaction of GO and bimetallic NPs resulted in significant stability over tested cycles.

In principle, removal efficiency decrease over tested cycles can be associated with (i) formation and thickening of the iron oxide layer due to Fe^0 and Fe^{2+} active sides oxidizing to Fe^{3+} (ii) loss of reaction site on the surface from tetracycline and intermediates physically block access therefore, hindering the reaction or iii) loss of metallic adsorbents due to dissolution especially in acidic mediums. Since iron oxide (Fe_3O_4) is also an excellent adsorbent for tetracycline and a range of pharmaceuticals, simply focusing on the oxidation state of iron or copper does not explain the increased stability of the adsorbent over 5 cycles. To further investigate the advantage of GO supported Fe/Cu over the unsupported nanoparticles the amount of metal leaching after batch experiment performed at pH 3 was measured using ICP-MS as shown in Figure 4-17.

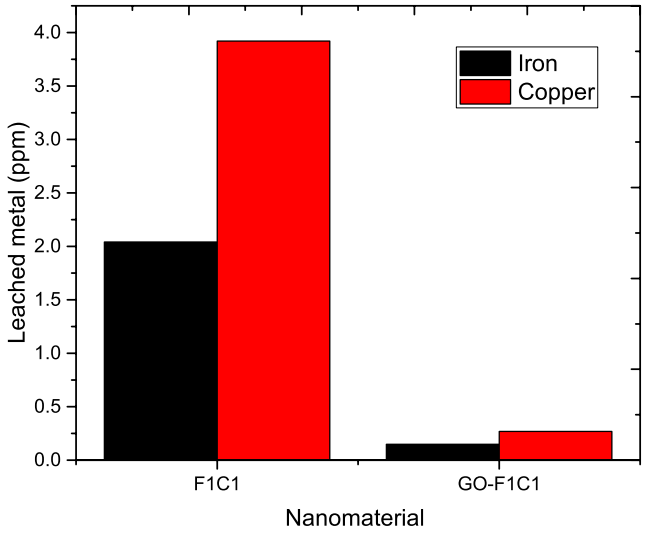

Figure 4-17: amount of copper and iron leached for Fe/Cu and GO supported Fe/Cu (conditions: pH 3, [TC]i=100 ppm, Time: 1 h, dosage=0.025 g L-1, rotatory shaker 250 rpm)

The leaching concentration of copper is higher than iron for both cases. Most importantly, depositing the nanoparticles on GO support reduced both iron and copper leaching by approximately 93%. This significant reduction in leaching can be attributed to the strong anchoring of Fe/Cu nanoparticles through F-O-C and Cu-O-C bonds [46, 85].Nanoparticles attached to GO surface have less exposed surface to the solution and therefore dissolve less than the loose nanoparticles [86, 87].

Increased stability of GO supported Fe/Cu can be explained by:

1) Decreased aggregation of Fe/Cu-GO comparing to Fe/Cu
2) Great dispersion of Fe/Cu nanoparticles on GO
3) Electron transfer between GO and Fe/Cu
4) Adsorption of TC on GO

The above claims can be supported by the literature. Iron and other nanoparticles supported on a solid matrix has shown less aggregation in comparison to unsupported nanoparticles. The presence of hydroxyl and epoxide groups on the surface of GO will aid GO supported nanoparticles to disperse easily in polar medium [65]. Homogenous dispersion of Fe/Cu

nanoparticles deposited on the surface and the edges of GO can be confirmed with TEM images. Abundance of functional groups on the surface of GO can result in great dispersion of nanoparticles instead of aggregated clusters. This structure can be beneficial in facilitating contaminant mass transfer towards the active sites. The increased surface area was confirmed during the BET experiment. However, it has been observed in TEM and confirmed by the literature that higher GO loading will result in a different composite structure. In this structure nanoparticles are sandwiched between layers of GO. This structure is not favored in reactions since the access to actives site will be reduced. Zubir et al.[49] reported a similar observation in which higher GO loading (>10%) resulted in agglomeration of Fe_3O_4 nanoparticles and consequently decline of AO7 degradation from 88 to 60%. Therefore, optimizing the GO loading is crucial to obtaining uniform dispersion of nanoparticles.

The third mechanism which is the electron transfer from GO to Fe/Cu, has been mentioned in several articles. GO consists of several unpaired π electrons, the presence of many semiconducting π -conjugated sp^2 carbon domains on its basal planes which are able to facilitate electron transfer between GO and Fe/Cu center via Fe-O-C bonds [47, 88], Jasujo et al. [47] reported the ability of TiO_2 decorated GO to transfer electrons between excited TiO_2 nanoparticles, they also reported an enhanced activity of nanocomposites as a result of GO's ability to store and transfer electrons. Zubir et al. [49] reported regeneration of Fe^{3+} on the surface of GO-Fe_3O_4 due to electron transfer from GO.

Although, removal of TC with GO particles was not observed in this work and high concentration of 100 ppm, several articles reported removal of TC with GO with an adsorption capacity of 330 mg g^{-1}. Liu et al. (2016) states that GO is a great adsorbent for antibiotics such as tetracycline but does not mention if GO by itself has a role in adsorbing TC when comparing removal capacity of GO-nZVI comparing to bare nZVI [46]. They further compare the pH behavior of the nanoparticle with those of mentioned by Ghadim et al. (2013) who reported partial removal of TC from 100 ppm TC solution [69]. Further experiments need to be done to determine the extent of GO role in adsorption of TC. This work recommends recovery of GO by increasing the pH which will result in separation of GO from the anchored nanoparticles and further desorbing the TC from the surface for quantification with LC-MS analysis [47, 89, 90].

Most importantly the metal leaching data is crucial in determining the toxicity of the adsorbent to the environment, for Fe/Cu-GO, both leached iron and copper concentrations are below the Canadian Health and Welfare standard of 1 ppm [59].

4.5.6 Desorption studies and transformation products

One of the important aspects of contaminant removal by adsorbents and catalyst processes is the formation of intermediates or transformation products (TP). These by products can be potentially more harmful than the parent product. In order to detect TPs for tetracycline, liquid chromatography-electrospray mass spectroscopy (LC-ESI-MS, Description : Agilent 1260 infinity equipped with simple quad G6120 MS) was performed. LC-ESI-MS with two different modes (positive and negative) performed and the retention time was used as a determining factor for choosing the analysis method. The first method by Chen et al. 2011[37] resulted in retention time of two minutes for tetracycline. Low retention time might decrease the accuracy of TP detection since some of the by-product's peaks might have a lower retention time than TC and consequently do not get detected in LC/MS. The second method by Yue et al. [91] resulted in a higher retention time of 13 minutes. TC has a molecular weight of 444.4 g mol^{-1} and a mass to charge (m/z) value of 443 on negative mode and 445 on positive mode.

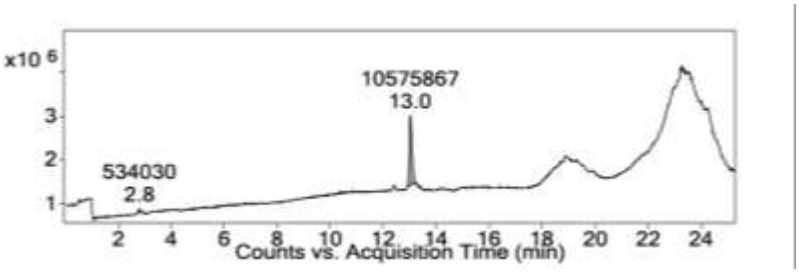

Figure 4-18: LC-MS spectra of TC (10 ppm) showing the retention time of 13 min positive ion mode

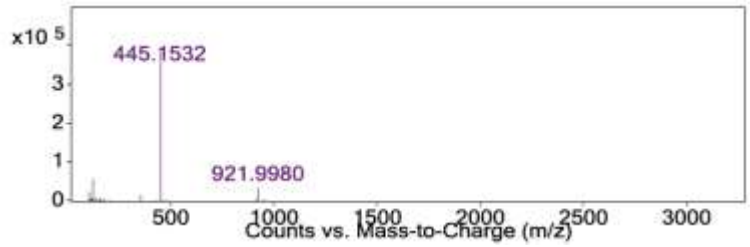

Figure 4-19: LC–MS spectra of TC (10 ppm) eluted at 13 min on positive mode

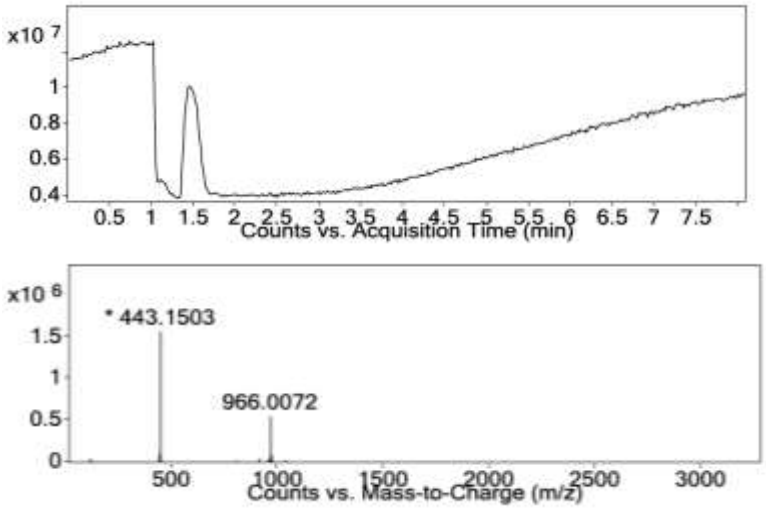

Figure 4-20: LC–MS spectra of TC (100 ppm) eluted at 1.5 min on negative mode with m/z of 443. The m/z of 966 is the peak corresponding to the correction ion

Desorption studies of tetracycline and by products from the adsorbent were performed using the method by Aslan et al. [44].

1) 10 ml of the aliquot was taken from the sample after 1 hour of the batch experiment
2) 100 µl of concentrated HCl were added to the 10 mL of sample aliquot and placed in a 25 mL vial
3) The vial was mixed for 3 minutes using a vortex mixer
4) The sample was then centrifuged at 8000 rpm for 10 minutes
5) The supernatant was collected and kept in the fridge for less than 24 h prior to LC-ESI-MS

In the first experiment running at optimum condition (pH 6.5, dosage 0.25 g L^{-1}, room temperature), a sample of effluent was separated and analyzed with LC-MS method. The effluent did not show any trace of TC or by-products. The prominent peak at m/z 966 is an ion used for internal calibration. These peaks are visible also for the pure TC sample (m/z of 966 in positive mode and 922 in negative mode). According to Keller et al. [92] and the Agilent manual ions at m/z of 121.05 and 922 for positive mode and m/z of 119.04 and 966 for negative mode are internal calibration standards. The most important aspect of the effluent analysis was to show almost complete removal of TC and by-products from the effluent.

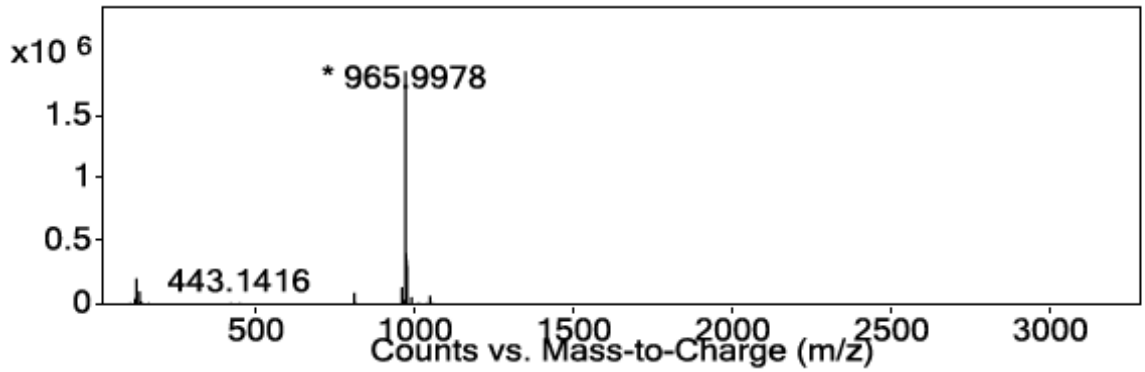

Figure 4-21: LC-MS spectra for TC supernatant after batch experiment (pH 6.5, [TC]i= 100 ppm, 0.25gL-1)

LS-ESI-MS data analysis were done according to these 3 steps:

1. Compare total ion chromatograms (TIC) of each sample and the tetracycline (TC) standard
2. Find compound TC by formula search ($C_{22}H_{24}N_2O_8$) (Table 4-5)
3. Extract ion chromatograms (EIC) of products of interest

Table 4-4: Compound TC species

TC Species	Calc *m/z*
$(M+H)^+$	445.1605
$(M+Na)^+$	467.1425
$(M+K)^+$	483.1164

$(2M+K)^+$	911.2958

For the positive ion electrospray (ESI), $[M+H]^+$ (molecular weight plus one proton) can be observed, $[M+k]^+$ and $[M+NA]^+$ can be observed for mobile phases containing an excess of 0.5 mmol of Na^+ and K^+. For higher analyte concentrations, protonated dimers $[2M+Na]^+$ can also be detected. Figure 4-19 shows the TIC for 10 ppm standard solution sample in comparison to analytes for pH 3.7 and 6.5. Two important observations can be made from this Figure 4-18, i) there was a peak shift for TC samples because of epimerization of TC; 2) other peaks are present because of TC degradation which are not present in the 10 ppm standard solution.

Figures A-4 to A-8 show the EIC comparison of effluent, analyte from the batch experiment performed at pH 3.7 and 6.5. From LC-ESI-MS, It is evident that most of the TC and by-products are not present in the influent meaning that the adsorbent not only adsorbed TC but also the by-products. In addition, there is a peak shift between TC standard samples and the analyte resulting from the epimerization of TC in weak acid environment from the desorption step. There is more degradation for pH 3.6 compared to pH 6.5 and most importantly adsorption is the main removal mechanism involved for removal of TC with Fe/Cu-GO nanohybrids. This observation agrees with Aslan et al.[44] who reported 58% recovery of TC from adsorbent with acid desorption with Cu/Fe NPs and claiming that major removal mechanism is due to the adsorption of TC to the NPs. Chen et al. [36] reported similar findings with PVP-nZVI mentioning adsorption as the leading removal mechanism for TC. Identifying degradation product is a challenging task since metal ions can form a bond with degradation products. This challenge is omnipresent in solid extraction of TC from soil or adsorbent since the degradation products can form a complex with metal ions present in the solution. Chen et al. [92] reported that presence of metal species such as Cu(II) can interfere with LC-MS data and effect the fate of TC in the environment[93, 94]. However, few essential peaks were identified and a degradation pathway can be hypothesized using the ion species and literature.

Aslan et al.[44] proposed a degradation pathway for Cu/Fe bimetallic nanoparticles. Our experiment differs from Aslan et al.[44] bimetallic Cu/Fe (core-shell vs. nanoalloy) and GO support of the nanoparticle. However, similar pathway has been suggested in presence of iron

and iron modified nanoparticles in different papers. All these articles suggest adsorption of tetracycline to the adsorbent surface and also reduction mechanism of TC degradation via core electron donation [16, 22, 36, 37, 44, 84].Therefore, based on the LC-MS results and similar findings a possible reaction mechanism is as follows:

Electrons will be produced via the following reactions;

Oxidation of iron in acidic solution:

$$Fe^0{}_{(s)} + 2\,H_2O \rightarrow Fe^{+2}_{(aq)} + 2OH^-_{(aq)} + H_{2(g)} + 2e^- \qquad (12)$$

Oxidation of iron in basic solution:

$$Fe^0{}_{(s)} + 2\,H^+_{(aq)} \rightarrow Fe^{+2}_{(aq)} + H_2 + 2e^- \qquad (13)$$

Produced electrons can reduce the functional groups in the following order:

1) Removal of methyl groups from dimethylamine at position A (See figure 4-22)
2) Removal of Hydroxyl group from position B
3) Removal of Amine group from position C

Then in the next stage:

4) Removal of hydroxyl groups from ring I, II, III (See figure 4-22)

Consequently:

5) Further removal of hydroxyl groups from ring I and III
6) Removal of ketone group from ring I

And eventually removal of other functional groups and ring cleavage.

Peak with m/z of 415, 174 and 194 were detected in all the samples. These peaks are in agreement with the proposed pathway by Fu et al. [84] for degradation of TC with nZVI. Degradation pathway of TC involves epimerization, dehydration, loss of functional groups and eventually cleavage of rings as shown in Figure 4-23.

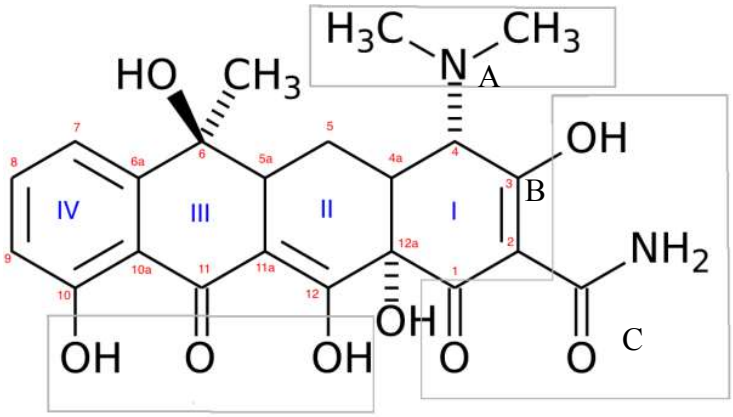

Figure 4-22: Molecular structure of TC showing functional groups

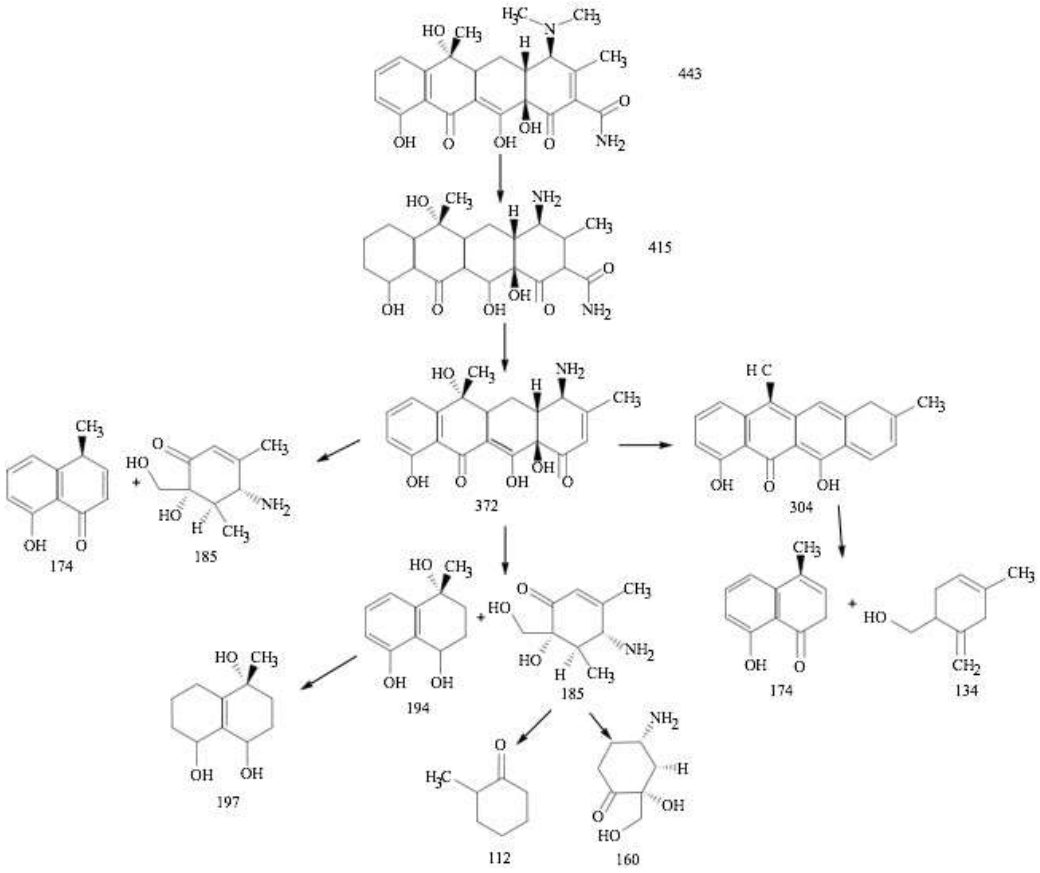

Figure 4-23: The proposed degradation pathway for TC showing possible reduction by-products with corresponding molecular weight (based on Fu et al. [84])

In conclusion, desorption studied show that the major removal mechanism of nanocomposite is by adsorption of TC or epimerization products. Nanocomposite not only removed TC but also removed transformation products from the solution. Degradation of TC is mainly due to loss of low energy functional groups with further degradation resulting in the loss of other functional groups and possibly ring cleavage. Since reduction by-products adsorb quickly to the nanocomposite the possibility of the formation of toxic by-products is lowered in aqueous matrices.

Chapter 5: Conclusion and Recommendations

This thesis focused on the development of the GO supported Fe/Cu NPs for removal of tetracycline from aqueous matrix. In this study, unique characteristics of the ex-situ deposited Fe/Cu nanoalloy were assessed. Overall performance of the nanocomposite was studied and the effect of pH and other experimental conditions on the removal performance was investigated. The stability of the synthesized magnetic nanocomposite was also assessed using the cyclic batch experiments as well as leaching measurements.

The first important finding is that the ex-situ deposition of Fe/Cu BNPs was successful and resulted in 58% increase in the BET surface area. XRD measurements confirmed the presence of both iron and copper on the surface of nanomaterial as well as the iron and copper oxide. TEM and SEM images showed a uniform deposition of BNPs on the surface of graphene oxide with possible sandwich like structure of GO and BNPs for higher GO loadings. EDS elemental mapping also confirmed the presence of carbon, copper and iron on the surface of the nanocomposite.

The key finding of this thesis was that GO proved to be a promising support for ex-situ immobilization of Fe/Cu BNPs. The synthesized nanocomposite removed almost 100% of TC from aqueous solution at optimum conditions. The removal is not highly pH dependent and GO supported nanocomposite shows a higher stability over Fe/Cu BNPs over 5 consecutive runs. Leaching of iron and copper is also reduced significantly as a result of GO support. Several hypotheses regarding the synergistic effect of copper and iron and also Fe/Cu BNP and the GO support was brought up in the results and discussion section that has been suggested by previous literature. The validity of these assumptions can be assessed via comprehensive research focusing on material aspect of the nanocomposite.

First of all, surface passivation of Fe/Cu and GO-Fe/Cu can be assessed using XPS. This study can confirm the decrease in oxidation of Fe and Cu species on the surface of GO-Fe/Cu nanocomposites as well as confirming the strong Fe-O-C bond between the anchored BNPs and the GO surface. This study can confirm the research hypothesis that the electron can be transferred from the GO surface to the BNPs for higher stability and durability of the nanocomposite. This bond has been observed by another study for in-situ deposition of iron on GO but this speculation needs to be confirmed for the ex-situ method [47].

In order to assess the applicability of this novel nanocomposite as an adsorbent, the effect of temperature and presence of competitive ions should be studied. Eventually, this nanocomposite could be used in pilot studies for removal of TC from synthetic, spiked or hospital wastewater. The major part of this research was done using UV-Vis spectrophotometer. However, for highly diluted antibiotic samples, it is recommended to use LC-ESI-MS as the measurement tool. LC-MS studies and the extraction of complexed TC from other wastewater contaminants can be very challenging. Therefore, a comprehensive study should focus on the complexing and chelating behavior of TC with other pollutants and heavy metals. Transformation products of TC removal must be carefully studied especially in the presence of chlorine to confirm that the toxic transformation products are not forming in this reaction. Leaching of copper and iron must be studied in real wastewater samples for consecutive runs and extreme conditions to confirm that the heavy metal leaching is not a major issue while using this nanocomposite.

In conclusion, ex-situ deposition of NPs on supports could be an interesting area of research. pH responsive and dynamic behavior of this system can be proven to be useful in developing and regenerating novel class of adsorbents and catalysts. The material aspect of nanocomposite and the exact reason lying behind the synergistic effect of iron/copper system and BNP and support system can be studied. The applicability aspect of these nanocomposites should be also studied comprehensively to assess the wide scale use of these nanocomposites in the future.

References

1. Sarmah, A.K., M.T. Meyer, and A.B.A. Boxall, *A global perspective on the use, sales, exposure pathways, occurrence, fate and effects of veterinary antibiotics (VAs) in the environment.* Chemosphere, 2006. **65**(5): p. 725-759.
2. Gao, P., Ding Y, Li H, Xargoraraki I., *Occurrence of pharmaceuticals in a municipal wastewater treatment plant: Mass balance and removal processes.* Chemosphere, 2012. **88**(1): p. 17-24.
3. Aga, D.S., O'Connor S, Ensley S, Payero JO, Snow D, Tarkalson D., *Determination of the Persistence of Tetracycline Antibiotics and Their Degradates in Manure-Amended Soil Using Enzyme-Linked Immunosorbent Assay and Liquid Chromatography−Mass Spectrometry.* Journal of Agricultural and Food Chemistry, 2005. **53**(18): p. 7165-7171.
4. Jacobsen, A.M.,Halling- Sørensen B, Ingerslev, Hansen SH., *Simultaneous extraction of tetracycline, macrolide and sulfonamide antibiotics from agricultural soils using pressurised liquid extraction, followed by solid-phase extraction and liquid chromatography–tandem mass spectrometry.* Journal of Chromatography A, 2004. **1038**(1–2): p. 157-170.
5. Dürckheimer, W., *Tetracyclines: Chemistry, Biochemistry, and Structure-Activity Relations.* Angewandte Chemie International Edition in English, 1975. **14**(11): p. 721-734.
6. Passarell, J.,Elizabeth L, Kathryn L, Alison K.M, Thaddeus H. Grasela., *Exposure–response analyses of tigecycline tolerability in healthy subjects.* Diagnostic Microbiology and Infectious Disease, 2009. **65**(2): p. 123-129.
7. Ding, Y. Zhang W, Gu C, Xagoraraki I, Li H., *Determination of pharmaceuticals in biosolids using accelerated solvent extraction and liquid chromatography/tandem mass spectrometry.* Journal of Chromatography A, 2011. **1218**(1): p. 10-16.
8. Watkinson, A.J., et al., *The occurrence of antibiotics in an urban watershed: From wastewater to drinking water.* Science of The Total Environment, 2009. **407**(8): p. 2711-2723.
9. Martínez, J.L., *Natural Antibiotic Resistance and Contamination by Antibiotic Resistance Determinants: The Two Ages in the Evolution of Resistance to Antimicrobials.* Frontiers in Microbiology, 2012. **3**: p. 1.
10. Kreuzig, R. and S. Höltge, *Investigations on the fate of sulfadiazine in manured soil: Laboratory experiments and test plot studies.* Environmental Toxicology and Chemistry, 2005. **24**(4): p. 771-776.
11. Kümmerer, K., *Antibiotics in the aquatic environment – A review – Part II.* Chemosphere, 2009. **75**(4): p. 435-441.
12. Kümmerer, K., *Antibiotics in the aquatic environment – A review – Part I.* Chemosphere, 2009. **75**(4): p. 417-434.
13. Hao, C., R. Clement, and P. Yang, *Liquid chromatography–tandem mass spectrometry of bioactive pharmaceutical compounds in the aquatic environment—a decade's activities.* Analytical and Bioanalytical Chemistry, 2007. **387**(4): p. 1247-1257.

14. Nassar, Nashaat N., *The application of nanoparticles for wastewater remediation*, in *Applications of Nanomaterials for Water Quality*. 2013, Future Science Ltd. p. 52-65.
15. Anjum, M., Rashid M., Muhammad W., Mohamed B.., *Remediation of wastewater using various nano-materials.* Arabian Journal of Chemistry.
16. Bagheri, H., A. Afkhami, and A. Noroozi, *Removal of Pharmaceutical Compounds from Hospital Wastewaters Using Nanomaterials: A Review.* Analytical and Bioanalytical Chemistry Research, 2016. **3**(1): p. 1-18.
17. Halling-Sørensen, B., G. Sengeløv, and J. Tjørnelund, *Toxicity of Tetracyclines and Tetracycline Degradation Products to Environmentally Relevant Bacteria, Including Selected Tetracycline-Resistant Bacteria.* Archives of Environmental Contamination and Toxicology, 2002. **42**(3): p. 263-271.
18. Hamscher, G., Silke S., Heinrich H., Heinz N., *Determination of Persistent Tetracycline Residues in Soil Fertilized with Liquid Manure by High-Performance Liquid Chromatography with Electrospray Ionization Tandem Mass Spectrometry.* Analytical Chemistry, 2002. **74**(7): p. 1509-1518.
19. Palm, G.J., Lederer T., Orth P, Saenger W, TakahashiM. Hillen W. Hinrichs W., *Specific binding of divalent metal ions to tetracycline and to the Tet repressor/tetracycline complex.* JBIC Journal of Biological Inorganic Chemistry, 2008. **13**(7): p. 1097.
20. Grenier, D., M.-P. Huot, and D. Mayrand, *Iron-Chelating Activity of Tetracyclines and Its Impact on the Susceptibility of Actinobacillus actinomycetemcomitans to These Antibiotics.* Antimicrobial Agents and Chemotherapy, 2000. **44**(3): p. 763-766.
21. Wang, G., Li-taoJ, Bo H., Yuhan S., *Self-assembled graphene monoliths: properties, structures and their pH-dependent self-assembly behavior.* New Carbon Materials, 2015. **30**(1): p. 30-40.
22. Guler, U.A., *Removal of tetracycline from aqueous solutions using nanoscale zero valent iron and functional pumice modified nanoscale zero valent iron.* Journal of Environmental Engineering and Landscape Management, 2016: p. 1-11.
23. Li, Y., T. Li, and Z. Jin, *Stabilization of Fe0 nanoparticles with silica fume for enhanced transport and remediation of hexavalent chromium in water and soil.* Journal of Environmental Sciences, 2011. **23**(7): p. 1211-1218.
24. Baym, M., Lieberman T. D. , Kelsic D. E. , Chaits, R., Rotem G., Ida., *Spatiotemporal microbial evolution on antibiotic landscapes.* Science, 2016. **353**(6304): p. 1147.
25. Fleming-Dutra, K.E., J. Am. Med. Assoc., 2016. **315**: p. 1864-1873.
26. O'Neil, J., *Antimicrobial Resistance: Tackling a crisis for the health and wealth of nations*. December, 2014, RAND EUROPE, KPMG: https://amr-review.org/.
27. Li, X.-Z. and H. Nikaido, *Efflux-Mediated Drug Resistance in Bacteria: an Update.* Drugs, 2009. **69**(12): p. 1555-1623.
28. Chang, Q., Wang W., Regev-Yochay G., Lipsitch M., Hanage P. W.., *Antibiotics in agriculture and the risk to human health: how worried should we be?* Evolutionary Applications, 2015. **8**(3): p. 240-247.
29. Kim, H.Y., Lee MJ, Yu SH. Kim SD., *The individual and population effects of tetracycline on Daphnia magna in multigenerational exposure.* Ecotoxicology, 2012. **21**(4): p. 993-1002.
30. Alexandre Augusto Borghi , M.S.A.P., *Tetracycline: Production, waste treatment and environmental impact assessment.* Brazilian Journal of Pharmaceutical Science, 2014. **50**(1): p. 25-40.

31. Topal, M., Senel G., Obek E, Topal A., , *Bioaccumulation of tetracycline and degradation products in Lemna gibba L. exposed to secondary effluents.* Desalination and Water Treatment, 2016. **57**(18): p. 8270-8277.
32. Homem, V. and L. Santos, *Degradation and removal methods of antibiotics from aqueous matrices – A review.* Journal of Environmental Management, 2011. **92**(10): p. 2304-2347.
33. Adams, C., et al., *Removal of antibiotics from surface and distilled water in conventional water treatment processes.* Journal of Environmental Engineering, 2002. **128**(3): p. 253-260.
34. Jiao, T., Liu Y., Wu Y., Zhang Q., Xuehai Y., *Facile and Scalable Preparation of Graphene Oxide-Based Magnetic Hybrids for Fast and Highly Efficient Removal of Organic Dyes.* Scientific Reports, 2015. **5**: p. 12451.
35. Choi, H., Al-Abed S., Agarwal S., *Synthesis of Reactive Nano-Fe/Pd Bimetallic System-Impregnated Activated Carbon for the Simultaneous Adsorption and Dechlorination of PCBs.* Chemistry of Materials, 2008. **20**(11): p. 3649-3655.
36. Hanay, Ö. and H. Türk, *Comprehensive evaluation of adsorption and degradation of tetracycline and oxytetracycline by nanoscale zero-valent iron.* Desalination and Water Treatment, 2015. **53**(7): p. 1986-1994.
37. Chen, H., Luo H., Lan Y., Dong T., *Removal of tetracycline from aqueous solutions using polyvinylpyrrolidone (PVP-K30) modified nanoscale zero valent iron.* Journal of Hazardous Materials, 2011. **192**(1): p. 44-53.
38. Stefaniuk, M., P. Oleszczuk, and Y.S. Ok, *Review on nano zerovalent iron (nZVI): From synthesis to environmental applications.* Chemical Engineering Journal, 2016. **287**: p. 618-632.
39. He, F., D. Zhao, and C. Paul, *Field assessment of carboxymethyl cellulose stabilized iron nanoparticles for in situ destruction of chlorinated solvents in source zones.* Water Research, 2010. **44**(7): p. 2360-2370.
40. He, L., Gong X., Ye L., Duan X., Yuan Y., *Synergistic effects of bimetallic Cu-Fe/SiO2 nanocatalysts in selective hydrogenation of diethyl malonate to 1,3-propanediol.* Journal of Energy Chemistry, 2016. **25**(6): p. 1038-1044.
41. Mukherjee, R., et al., *A review on synthesis, characterization, and applications of nano zero valent iron (nZVI) for environmental remediation.* Critical Reviews in Environmental Science and Technology, 2016. **46**(5): p. 443-466.
42. Duan, S. and R. Wang, *Bimetallic nanostructures with magnetic and noble metals and their physicochemical applications.* Progress in Natural Science: Materials International, 2013. **23**(2): p. 113-126.
43. Reddy, A.V.B., Yusop Z., Jaafar J., Gajulapalle M., *Recent progress on Fe-based nanoparticles: Synthesis, properties, characterization and environmental applications.* Journal of Environmental Chemical Engineering, 2016. **4**(3): p. 3537-3553.
44. Aslan, S., et al., *Removal of tetracyclines from aqueous solution by nanoscale Cu/Fe bimetallic particle.* Desalination and Water Treatment, 2016. **57**(31): p. 14762-14773.
45. Luo, L., Dai C., Zhang A., Wang Jm Liu M., *A facile strategy for enhancing FeCu bimetallic promotion for catalytic phenol oxidation.* Catalysis Science & Technology, 2015. **5**(6): p. 3159-3165.

46. Liu, W., MaJ., Wen Y., Liu E., *A pH-responsive and magnetically separable dynamic system for efficient removal of highly dilute antibiotics in water.* Water Research, 2016. **90**: p. 24-33.
47. Zubir, N.A., Yacou C., MotuzasJ., Zhang X., *Structural and functional investigation of graphene oxide–Fe3O4 nanocomposites for the heterogeneous Fenton-like reaction.* Scientific Reports, 2014. **4**: p. 4594.
48. Lam, F.L.Y. and X. Hu, *pH-Insensitive Bimetallic Catalyst for the Abatement of Dye Pollutants by Photo-Fenton Oxidation.* Industrial & Engineering Chemistry Research, 2013. **52**(20): p. 6639-6646.
49. Zubir, N.A., Motuzas J., Yacou C., ZhangX., *Graphene oxide with zinc partially substituted magnetite (GO-Fe1-xZnxOy) for the UV-assisted heterogeneous Fenton-like reaction.* RSC Advances, 2016. **6**(50): p. 44749-44757.
50. Gao, Y.,Li Y., Zhang L., Huang Y., Hu J Shah SM., *Adsorption and removal of tetracycline antibiotics from aqueous solution by graphene oxide.* Journal of Colloid and Interface Science, 2012. **368**(1): p. 540-546.
51. Aliofkhazraei, M. and A.S.H. Makhlouf, *Handbook of nanoelectrochemistry : electrochemical synthesis methods, properties, and characterization techniques.* 2016.
52. Han, Z., Y. Dong, and S. Dong, *Copper–iron bimetal modified PAN fiber complexes as novel heterogeneous Fenton catalysts for degradation of organic dye under visible light irradiation.* Journal of Hazardous Materials, 2011. **189**(1–2): p. 241-248.
53. Wang, J., Liu C., Tong L., Li J., Luo R., *Iron-copper bimetallic nanoparticles supported on hollow mesoporous silica spheres: an effective heterogeneous Fenton catalyst for orange II degradation.* RSC Advances, 2015. **5**(85): p. 69593-69605.
54. Wang, J., et al., *Iron-copper bimetallic nanoparticles supported on hollow mesoporous silica spheres: the effect of Fe/Cu ratio on heterogeneous Fenton degradation of a dye.* RSC Advances, 2016. **6**(59): p. 54623-54635.
55. Fan, B., et al., *Oxidation of cyclohexane over iron and copper salen complexes simultaneously encapsulated in zeolite Y.* Applied Catalysis A: General, 2008. **340**(1): p. 67-75.
56. Xia, M., et al., *A highly active bimetallic oxides catalyst supported on Al-containing MCM-41 for Fenton oxidation of phenol solution.* Applied Catalysis B: Environmental, 2011. **110**: p. 118-125.
57. Karlsson, H.L., et al., *Copper Oxide Nanoparticles Are Highly Toxic: A Comparison between Metal Oxide Nanoparticles and Carbon Nanotubes.* Chemical Research in Toxicology, 2008. **21**(9): p. 1726-1732.
58. Griffitt, R.J., et al., *Effects of particle composition and species on toxicity of metallic nanomaterials in aquatic organisms.* Environmental Toxicology and Chemistry, 2008. **27**(9): p. 1972-1978.
59. Agency, E.P. *2016 Draft Estuarine/Marine Copper Aquatic Life Ambient Water Quality Criteria*. 2016 [cited 2017].
60. Ou, L., et al., *Toxicity of graphene-family nanoparticles: a general review of the origins and mechanisms.* Particle and Fibre Toxicology, 2016. **13**(1): p. 57.
61. Lalwani, G., et al., *Toxicology of graphene-based nanomaterials.* Advanced Drug Delivery Reviews, 2016. **105, Part B**: p. 109-144.

62. Jamei, M.R., M.R. Khosravi, and B. Anvaripour, *Investigation of ultrasonic effect on synthesis of nano zero valent iron particles and comparison with conventional method.* Asia-Pacific Journal of Chemical Engineering, 2013. **8**(5): p. 767-774.
63. Morales-Luckie, R.A., et al., *One-step aqueous synthesis of stoichiometric Fe–Cu nanoalloy.* Materials Letters, 2008. **62**(26): p. 4195-4197.
64. Yedra, A., et al., *Nanoscale alloys prepared by sodium borohydride reduction of aqueous Fe–Cu and Co–Cu solutions.* Journal of Magnetism and Magnetic Materials, 2003. **254–255**: p. 14-16.
65. Konios, D., et al., *Dispersion behaviour of graphene oxide and reduced graphene oxide.* Journal of Colloid and Interface Science, 2014. **430**: p. 108-112.
66. Rittermeier, A., et al., *The formation of colloidal copper nanoparticles stabilized by zinc stearate: one-pot single-step synthesis and characterization of the core-shell particles.* Physical Chemistry Chemical Physics, 2009. **11**(37): p. 8358-8366.
67. de Faria, A.F., et al., *Anti-adhesion and antibacterial activity of silver nanoparticles supported on graphene oxide sheets.* Colloids Surf B Biointerfaces, 2014. **113**: p. 115-24.
68. Lin, Y., S. Xu, and J. Li, *Fast and highly efficient tetracyclines removal from environmental waters by graphene oxide functionalized magnetic particles.* Chemical Engineering Journal, 2013. **225**: p. 679-685.
69. Ghadim, E.E., et al., *Adsorption Properties of Tetracycline onto Graphene Oxide: Equilibrium, Kinetic and Thermodynamic Studies.* PLoS ONE, 2013. **8**(11): p. e79254.
70. Timofeeva, M.N., et al., *The effect of Fe/Cu ratio in the synthesis of mixed Fe,Cu,Al-clays used as catalysts in phenol peroxide oxidation.* Applied Catalysis B: Environmental, 2009. **90**(3–4): p. 618-627.
71. Lai, B., et al., *Removal of p-nitrophenol (PNP) in aqueous solution by the micron-scale iron–copper (Fe/Cu) bimetallic particles.* Applied Catalysis B: Environmental, 2014. **144**: p. 816-830.
72. Huang, Q., et al., *Tunable Synthesis and Immobilization of Zero-Valent Iron Nanoparticles for Environmental Applications.* Environmental Science & Technology, 2008. **42**(23): p. 8884-8889.
73. Wang, Y.-J., et al., *Adsorption and Cosorption of Tetracycline and Copper(II) on Montmorillonite as Affected by Solution pH.* Environmental Science & Technology, 2008. **42**(9): p. 3254-3259.
74. Foo, K.Y. and B.H. Hameed, *Insights into the modeling of adsorption isotherm systems.* Chemical Engineering Journal, 2010. **156**(1): p. 2-10.
75. Hanay, Ö., et al., *Removal of tetracycline and oxytetracycline by microscale zerovalent iron and formation of transformation products.* Environmental Science and Pollution Research, 2014. **21**(5): p. 3774-3782.
76. Dai, J., et al., *Preparation of molecularly imprinted nanoparticles with superparamagnetic susceptibility through atom transfer radical emulsion polymerization for the selective recognition of tetracycline from aqueous medium.* Journal of Hazardous Materials, 2012. **205-206**: p. 179-188.
77. Oladoja, N.A., et al., *Preparation of magnetic, macro-reticulated cross-linked chitosan for tetracycline removal from aquatic systems.* Colloids and Surfaces B: Biointerfaces, 2014. **117**: p. 51-59.
78. Yang, X., et al., *Preparation of ferric-activated sludge-based adsorbent from biological sludge for tetracycline removal.* Bioresource Technology, 2016. **211**: p. 566-573.

79. Zhang, M., et al., *Effect of pore size distribution on tetracycline adsorption using magnetic hypercrosslinked resins.* Microporous and Mesoporous Materials, 2014. **184**: p. 105-111.
80. Zhou, Q., et al., *Efficient removal of tetracycline by reusable magnetic microspheres with a high surface area.* Chemical Engineering Journal, 2012. **210**: p. 350-356.
81. Liu, Q., et al., *Removal of tetracycline from aqueous solution by a Fe3O4 incorporated PAN electrospun nanofiber mat.* Journal of Environmental Sciences, 2015. **28**: p. 29-36.
82. Zhang, Y., et al., *Removal of tetracycline and oxytetracycline from water by magnetic Fe3O4@graphene.* Environmental Science and Pollution Research, 2017. **24**(3): p. 2987-2995.
83. Rivera-Utrilla, J., et al., *Tetracycline removal from water by adsorption/bioadsorption on activated carbons and sludge-derived adsorbents.* Journal of Environmental Management, 2013. **131**: p. 16-24.
84. Fu, Y., et al., *High efficient removal of tetracycline from solution by degradation and flocculation with nanoscale zerovalent iron.* Chemical Engineering Journal, 2015. **270**: p. 631-640.
85. Khusnun, N.F., et al., *Interaction between copper and carbon nanotubes triggers their mutual role in the enhanced photodegradation of p-chloroaniline.* Physical Chemistry Chemical Physics, 2016. **18**(17): p. 12323-12331.
86. Pirkanniemi, K. and M. Sillanpää, *Heterogeneous water phase catalysis as an environmental application: a review.* Chemosphere, 2002. **48**(10): p. 1047-1060.
87. Soon, A.N. and B.H. Hameed, *Heterogeneous catalytic treatment of synthetic dyes in aqueous media using Fenton and photo-assisted Fenton process.* Desalination, 2011. **269**(1–3): p. 1-16.
88. Jasuja, K., et al., *Microwave-Reduced Uncapped Metal Nanoparticles on Graphene: Tuning Catalytic, Electrical, and Raman Properties.* The Journal of Physical Chemistry Letters, 2010. **1**(12): p. 1853-1860.
89. Fan, W., et al., *Hybridization of graphene sheets and carbon-coated Fe3O4 nanoparticles as a synergistic adsorbent of organic dyes.* Journal of Materials Chemistry, 2012. **22**(48): p. 25108-25115.
90. Zeng, T., et al., *A novel Fe3O4-graphene-Au multifunctional nanocomposite: green synthesis and catalytic application.* Journal of Materials Chemistry, 2012. **22**(35): p. 18658-18663.
91. Yue, Z., et al., *Determination of Multi-Residues of Tetracyclines and Their Metabolites in Milk by High Performance Liquid Chromatography-Tandem Positive-ion Electrospray Ionization Mass Spectrometry.* Chinese Journal of Analytical Chemistry, 2006. **34**(9): p. 1255-1259.
92. Keller, B.O., et al., *Interferences and contaminants encountered in modern mass spectrometry.* Analytica Chimica Acta, 2008. **627**(1): p. 71-81.
93. O'Connor, S., J. Locke, and D.S. Aga, *Addressing the challenges of tetracycline analysis in soil: extraction, clean-up, and matrix effects in LC-MS.* Journal of Environmental Monitoring, 2007. **9**(11): p. 1254-1262.
94. Chen, W.-R. and C.-H. Huang, *Transformation of Tetracyclines Mediated by Mn(II) and Cu(II) Ions in the Presence of Oxygen.* Environmental Science & Technology, 2009. **43**(2): p. 401-407.
95. Babaee, F.Y., *Removal of Arsenic from Water and Immobilization in Soil*

Using Iron/Copper Nanoparticle, in *Department of Building, Civil and Environmental Engineering*. May 2016, Concordia University.

Appendix

In this section, supplementary data and graphs are provided for better understanding of the information presented in the thesis.

A.1 XRD

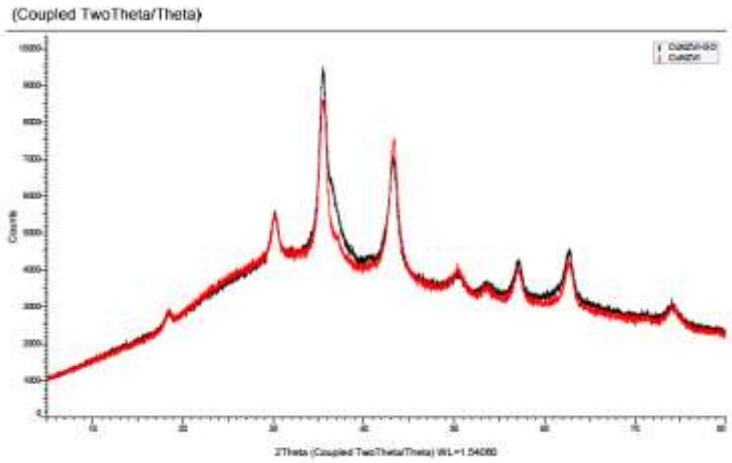

Figure A-0-1: Overlaid XRD spectra for Cu/Fe BNPs and supported Cu/Fe BNPs

Table 0-1: Corresponding peak to each 2-theta value and JCPDS card number

2-Theta	Corresponding peak	JCPDS Card Number	
20.4	a-Fe_2O_3 (hematite)	033-0664	
33.2	a-Fe_2O_3 (hematite)	033-0664	Magnetite 220
36.4	Fe_3O_4 and γ-Fe_2O_3	001-1223 82-1533	Magnetite 311
36.5	Cu_2O	5-0667	cubic Cu_2O(111)
43.2	Cu	04–0836	fcc Cu(111)
44.4	Fe	06-0696	Fcc Fe(110)
50.82	Cu	04–0836	Cu 200
53.6	Magnetite	82-1533	Magnetite 422
59	Magnetite	82-1533	Magnetite 400
64	Cu-O Fe	82-1533	Fe 200
74.5	Cu	04–0836	Cu 220

A.2 Calibration curve

A sample calibration obtained by UV-Vis for Tetracycline at 357.6 nm.

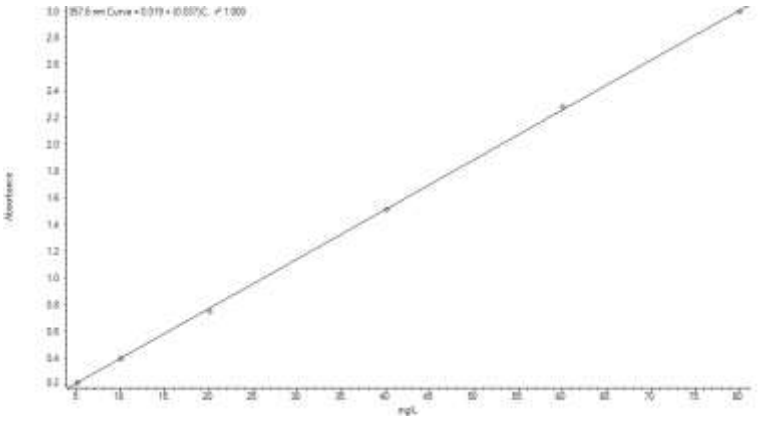

Figure A-2: Calibration Curve for Tetracycline at 357.6 nm

A.3 Zeta Potential

The zeta (ζ) potential of the stabilized Fe/Cu nanoparticles (0.04% w/w starch) was measured using a Zeta Potential/Particle Size Analyzer (BrookHaven Instrument Corp., ZetaPlus / Bl-PALS, Holtsville, NY) at a 173° scattering angle with two replicates. Fe/Cu BNPs show zero point of charge value at pH between 8 and 9. This experiment was performed by Dr. Babaee [95].

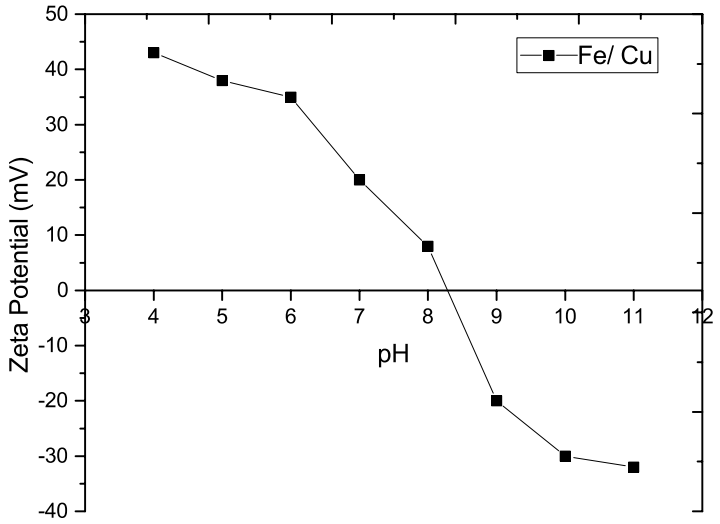

Figure A-3: Zeta potential for Fe/Cu nanoparticles

A.4 Determining the optimum Copper/Iron ratio

Determining the right molar ratio for copper and iron is crucial for maximum stability and performance. 3 bimetallic nanoparticles were synthesized and tested. Based on leaching values and performance, F1C1 was chosen for further experiments.

Table A-2: Determining the optimum copper to iron ratio

Sample ID	**Iron Salt concentration (mM)**	**Copper Salt concentration (mM)**	**Theoretical Iron wt%**	**Theoretical Copper wt%**	**Iron leaching(mg/L)**	**Copper leaching(mg/L)**	**% removal**
F3C1	7.5	2.5	67	33	1.12	5.68	100%
F1C1	5	5	50	50	2.04	3.92	100%
F1C3	2.5	7.5	33	67	1.53	11.2	90%

A.5 LC-ESI-MS

Detailed method of LC-ESI-MS is as follows:

Column: Agilent Eclipse Plus C 8 (4.6 x 100 mm; 3.5 µm)

Mobile phase **A**: Water + 0.1% Formic acid

Mobile phase **B**: Methanol+ 0.1% Formic acid

Flow rate: 0.7 ml/min
Gradient:

Table A-3: Gradient of mobile phase for LC-ESI-MS

Time	**% Methanol**
0	5
10	40
11	40
13	65
18	95
20	95

LC-ESI-MS parameters:

Positive mode; *m/z* 100-3200; source temp - 350 °C; source drying N_2 - 12 l/min; ion spray 4000 V; frag 100 V

TIC scans and EIC comparisons for effluent, batch experiment performed at pH 3.7 and 6.5 are shown below:

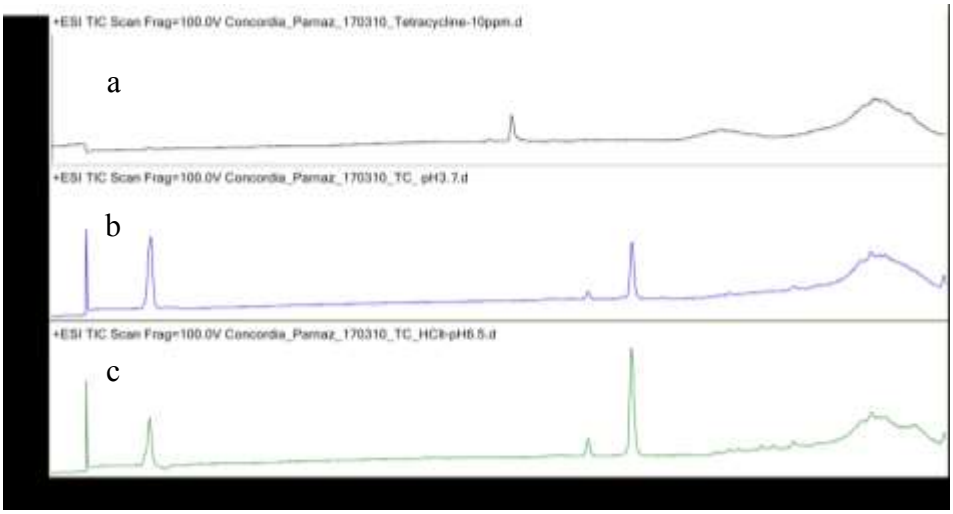

Figure A-4: TIC comparison for (a) TC 10 ppm (b) desorbed TC and by products after batch experiment under optimum condition at pH 3.7, (c) desorbed TC and by products after batch experiment under optimum condition at pH 6.5

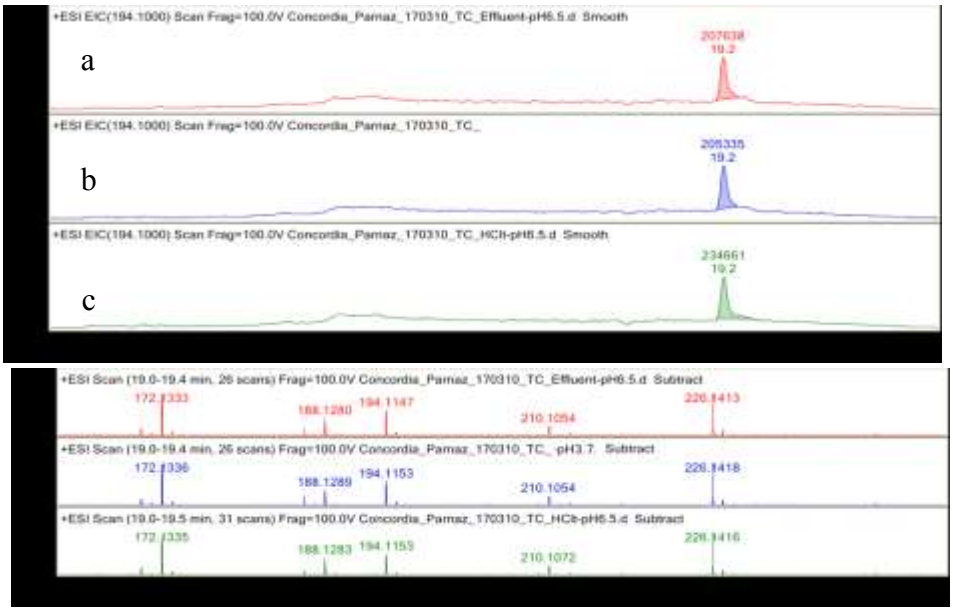

Figure A-5: EIC for m/z 134 for (a) Batch experiment supernatant at pH 6.5(b) desorbed batch experiment pH 3.7 (c) desorbed batch experiment at pH 6.5

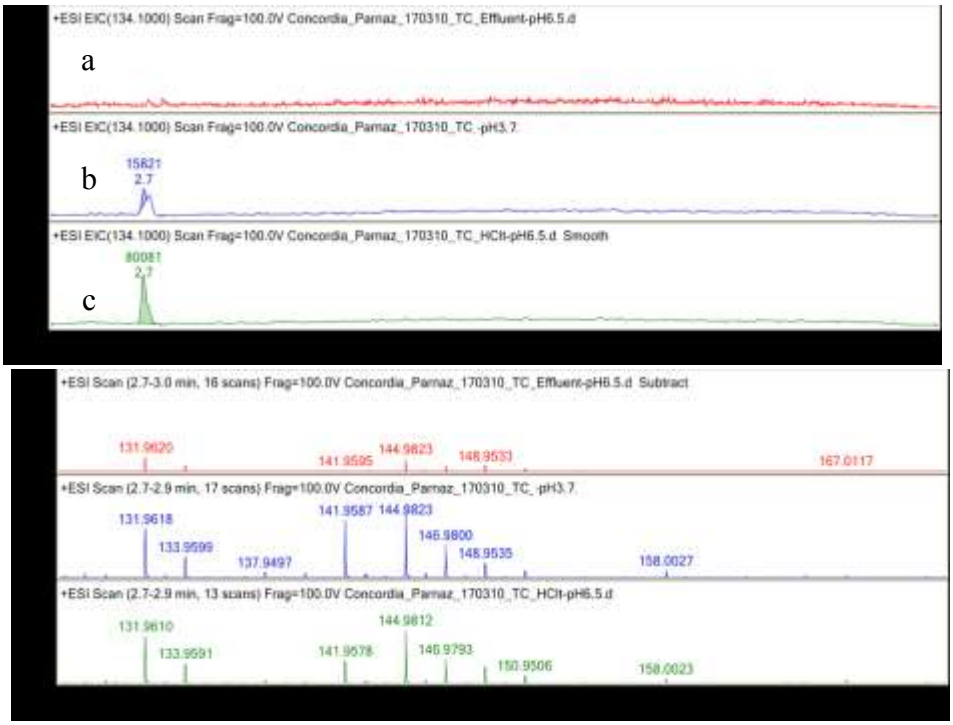

Figure A-6: EIC for m/z 196 for (a) Batch experiment supernatant at pH 6.5 (b) desorbed batch experiment pH 3.7, (c) desorbed batch experiment at pH 6.5

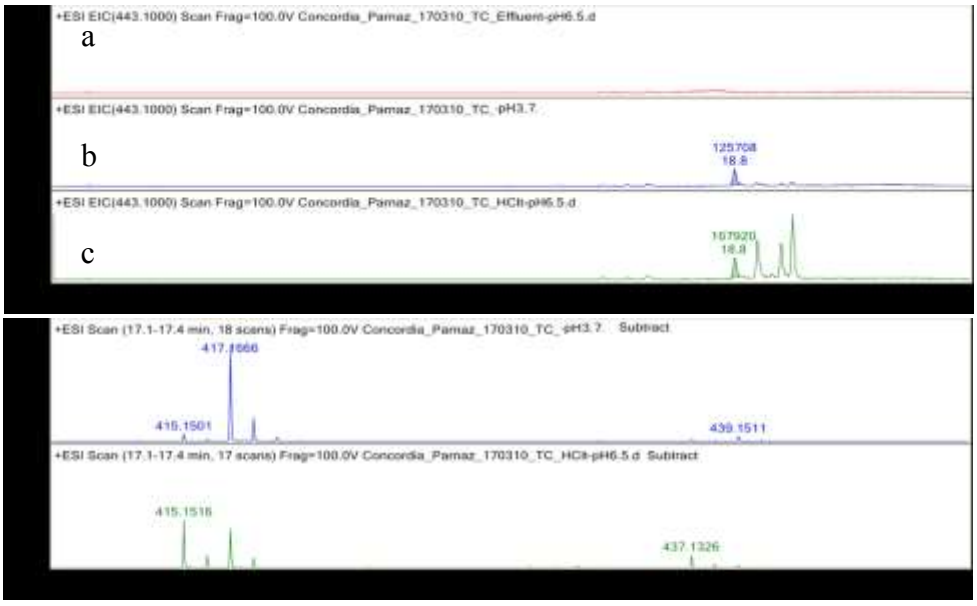

Figure A-7: EIC for m/z 415 for (a) Batch experiment supernatant at pH 6.5, (b) desorbed batch experiment pH 3.7, (c) desorbed batch experiment at pH 6.5

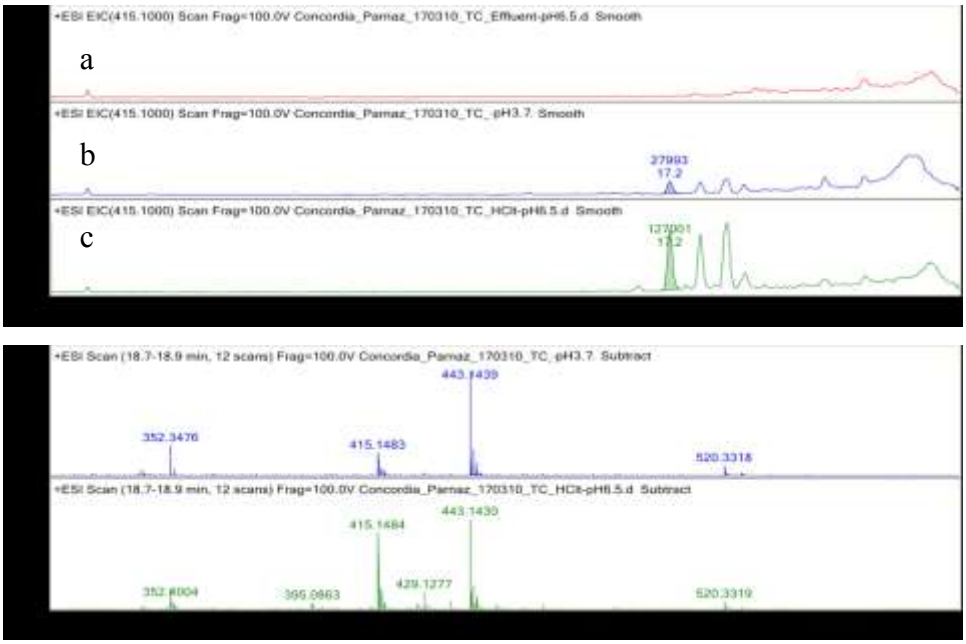

Figure A-8: EIC for m/z 443 for (a) TC effluent, (b) desorbed batch experiment pH 3.7, (c) desorbed batch experiment at pH 6.5

A.6 Sample of UV-Vis overlaid spectra

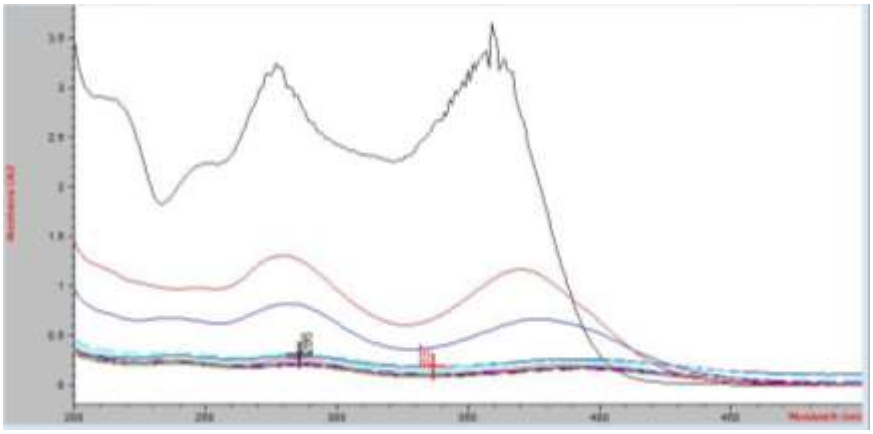

Figure A-9: Sample overlaid UV-Vis spectra (pH=6.5 unadjusted conditions: [TC]i=100 ppm, dosage= 0.05, UV range: 200-500 nm)